UiT The Arctic University of Norway

Faculty of Health Sciences

Department of Pharmacy, UiT – the Arctic University of Norway, and

Department of Pharmaceutical Technology and Biopharmacy Research Group, Albert-Ludwigs University of Freiburg

Process optimization of albumin-stabilized mitotane nanoparticle preparation by dual centrifugation and first lyophilization study

Cindy Jia Ru Zhang

Master's thesis (FAR-3911) in Pharmacy 2021/2022

Supervisor: PhD student Carolin Langer (Albert-Ludwigs University of Freiburg)

Co-supervisor: Professor Nataša Škalko-Basnet (the Arctic University of Norway)

Master's thesis for MPharm degree of Pharmacy

Process optimization of albumin-stabilized mitotane nanoparticle preparation by dual centrifugation and first lyophilization study

by

Cindy Jia Ru Zhang

May 2022

SUPERVISOR

PhD student Carolin Langer (Albert-Ludwigs University of Freiburg)

E-mail address: carolin.langer@pharmazie.uni-freiburg.de

CO-SUPERVISOR

Professor Nataša Škalko-Basnet (the Arctic University of Norway)

E-mail address: natasa.skalko-basnet@uit.no

Department of Pharmaceutical Technology and Biopharmacy

Institute of Pharmaceutical Sciences

Albert-Ludwigs University of Freiburg

Faculty of Health Sciences

Department of Pharmacy

UiT – the Arctic University of Norway

Acknowledgement

The work associated with this master's thesis was carried out as a part of the research group in the department of Pharmaceutical Technology and Biopharmacy at the Albert-Ludwigs-University of Freiburg from October 2021 to May 2022.

First of all, I would like to express my gratitude to my supervisors, Carolin Langer (Department of Pharmaceutical Technology and Biopharmacy, Albert-Ludwig University of Freiburg) and Professor Nataša Škalko-Basnet (Department of Pharmacy, UiT – the Arctic University of Norway), for taking time to advice me, guide me, and to give me feedback. You have helped me a lot and taught me so much throughout my project. Thank you.

I would also like to express my gratitude to Prof. Dr. Regine Süss for making this exchange happen. Thank you for accepting my application and for assigning me a supervisor that allowed me to complete my master's thesis here in Freiburg as a part of your team.

Furthermore, I would like to thank Marte Foss Tveiten, Mathias Eriksen and Janne Erikke Mjelle from the Department of Pharmacy at UiT – the Arctic University of Norway for also making this exchange possible.

I would like to thank everyone else in the research group from the Department of Pharmaceutical Technology and Biopharmacy for helping me out whenever I needed it, and for welcoming me. Thanks to PhD students, Laurine Kaul, and Anna Ruppl, for helping and answering my questions regarding the lyophilization. And although the experiment did not take place, I would also like to thank PhD student Laurens Kersch for finding time to help me learn more about photostability testing. Also, a special thanks to Monika Köll-Weber for your assistance in the lab and for never giving up trying to find the answers I was seeking.

Finally, I would like to thank my friends. Thanks to Emilie Luu for you support and being a video-call away. A big thanks to Linda Kourng, for accompanying me to Freiburg. Thank you for being there for me and lending me a hand whenever I needed it. I could not have gone on this journey without you.

Table of contents

Acknowledgement III

Table of contents IV

Abstract VII

List of tables VIII

List of figures VIII

List of abbreviations XI

1 Introduction 1

1.1 The role of mitotane in treatment of adrenocortical carcinoma 1

1.1.1 What is adrenocortical carcinoma? *2*

Management of adrenocortical carcinoma 3

1.1.2 What is mitotane? *4*

Pharmacological aspects of Mitotane 4

Pharmacokinetic properties 4

Pharmacodynamic properties 5

Mechanism of action *5*

Clinical limitations 5

1.2 Formulation development for mitotane 6

1.2.1 Nanoformulation as a potential formulation for parenteral administration. *6*

Nanotechnology and nanoparticle systems 6

Utilizing albumin as a nanocarrier for drug delivery 9

The potential of albumin-based nanocarrier 10

Bovine serum albumin vs. human serum albumin *13*

1.3 Dual centrifugation as a method to produce nanoparticles 14

1.3.1 Principles of dual centrifugation *14*

1.4 Lyophilization for improved stability 16

1.4.1 Principle of lyophilization *18*

Stages of freeze-drying process 19
Freezing stage 19
Primary drying 20
Secondary drying 22
Addition of cryo- and lyoprotectant 22
Lyophilized drug product – cake appearance 24

2 Aim of the study 25

3 Materials, equipment, and instruments 26

3.1 Materials 26

3.1.1 Chemicals 26

3.1.2 Equipment 27

3.1.3 Protective clothing and equipment 28

3.2 Instruments 28

4 Methods 30

4.1 Process optimization of nab-mitotane preparation by dual centrifugation 30

4.1.1 Preparing stock solutions 30

4.1.2 Step 1: Dual centrifugation 31

4.1.3 Step 2: the cross-linking step 33

4.1.4 Step 3: Purification of the nanoparticles 34

4.1.5 Step 4: Determination of particle size and size distribution 34

4.2 Lyophilization for stability improvement of nab-mitotane 35

4.2.1 Short-term stability study 35

4.2.2 Step 1: Preparing sucrose stock solution and samples for lyophilization 36

4.2.3 Step 2: The lyophilization process of nab-mitotane 37

4.2.4 Step 3: Preparation of the samples for storage 38

4.2.5 Step 4A: Reconstitution of the freeze-dried nab-mitotane 39

4.2.6 Step 4B: Determination of particle size and size distribution 39

4.2.7 Evaluation of lyophilized cake appearance 40

4.2.8 Evaluation of particle size and polydispersity 40

4.3 Statistical analysis....41

5 Results and discussion....42

5.1 Dual centrifugation – particle size and size distribution....42

5.1.1 The influence of ceramic beads on the particle size....42

The influence of different amounts of beads....42

The influence of ceramic bead size....44

5.1.2 The influence of temperature on particle size....46

5.1.3 The influence of processing time on particle size....48

5.1.4 The influence of pH on particle size....50

5.1.5 Dual centrifugation method optimization – summary....51

5.2 Lyophilization – cake appearance, particle size and size distribution....51

5.2.1 The cake appearance of lyophilized product over time....52

5.2.2 Particle size and size distribution....54

Before and after lyophilization....55

Stability after storage at room- and refrigerated temperature....56

The effect of different storage temperature on the stability....57

5.2.3 Short-term stability study – summary....59

6 Conclusion and future work....60

7 References....61

8 Appendix....68

The influence of different amounts of ceramic beads on particle size....69

The influence of temperature on the particle size....69

The influence of different sucrose concentrations on the particle size....71

Stability after storage at room temperature....72

Abstract

Albumin-stabilized mitotane nanoparticles intended for intravenous application can serve as a potential formulation for the treatment of adrenocortical carcinoma. However, the particle size of a nanoparticle-based formulation is crucial for the in vivo behavior of the nanoparticles following an intravenous injection. Prior to this project, the particle size of this nanoformulation had a mean of approximately 350 nm. Therefore, there is a need of a process optimization of albumin-stabilized mitotane nanoparticle preparation. The preparation of these nanoparticles was conducted by the method of dual centrifugation. In addition to this, lyophilization was carried out to get a first knowledge on how the particle size of the albumin-stabilized mitotane nanoparticles could be influenced by the process, as well as the influence of storing the freeze-dried product over a short period of time.

By varying different parameters such as the processing temperature and processing time for the DC, as well as using different sizes and amounts of ceramic beads as homogenization aid, and finally by using BSA solution adjusted to different pH, a reduced mean particle size was accomplished.

The results of the short-term stability study concluded the possibility of obtaining stable albumin-stabilized mitotane nanoparticles following the lyophilization process. Additionally, the nanoparticles in terms of particle size remained unchanged upon storage at refrigerated temperature. However, storage at room temperature need further investigation.

Keywords: mitotane; albumin; dual centrifugation; adrenocortical carcinoma; lyophilization; stability

List of tables

Table 1.1: *Examples of the mechanisms of action. 5*

Table 3.1: *List of chemicals used in this project 26*

Table 3.2: *List of equipment, containers and other supplies used in this project. 27*

Table 3.3: *List of protective clothing and equipment 28*

Table 3.4: *List of instruments used in this project 28*

Table 4.1: *Comparison between different sizes of ceramic beads in addition to different amounts of ceramic beads. 32*

Table 4.2: *A) Comparison of different temperatures. B) Comparison of different processing time. 32*

Table 4.3*: Comparison between BSA solutions of different pH. 33*

Table 4.4: *The statistical tests that were used on the different experiments for comparison. 41*

List of figures

Figure 1.1*: Adrenocortical carcinoma occurring in cortex of the adrenal glands. Created on BioRender.com. 2*

Figure 1.2: A) *The chemical structure of o,p'-DDT.* ***B)*** *The chemical structure o,p'-DDD, also commonly known as mitotane. Created on PubChem Sketcher V2.4. ..... 4*

Figure 1.4: *Size comparison between a nanoparticle, a soccer ball and planet earth. The difference in size between a nanoparticle and a soccer ball is the same as the difference in size between the soccer ball and earth [32]. 7*

Figure 1.5: *Examples of various types of nanocarrier systems. Created with BioRender.com. 8*

Figure 1.6: *A schematic representation of a targeted liposomal drug delivery system. Created with BioRender.com. 8*

Figure 1.7: *A summary of potential advantages with an injectable dosage form in comparison to an oral dosage form [5] 9*

Figure 1.8: *Advantages of albumin-based nanoparticles. Created with BioRender.com. 10*

Figure 1.9: *A) Normal blood vessel. B) Leaky blood vessel at tumor site. C) Accumulation of albumin-stabilized drug nanoparticle at tumor site through transcytosis [44, 45]. 12*

Figure 1.10: *Structures of* ***A)*** *BSA and of* ***B)*** *HSA. Created with BioRender.com, PDB ID 4F5S (BSA) and 7DJN (HSA). 12*

Figure 1.11: A) *The set-up of dual centrifuge ZentriMix 380 R with a major (main) rotation and sample (secondary) rotation. The sample vials are placed into the secondary dual rotor in horizontal orientation. Photo:*

Cindy Zhang. ***B)*** *Set-up with sample vials placed into the secondary dual rotor in vertical orientation. Photo: Cindy Zhang.* ***C)*** *Schematic view of vertical and horizontal vial orientation. Modified from [48]. 15*

Figure 1.12*:* ***A)*** *stable suspension – a uniform dispersion of particles.* ***B-D)*** *unstable suspensions – aggregation and agglomeration in which particles stick to each other, likely followed by sedimentation. Created with BioRender.com 17*

Figure 1.13: A) *Christ® Alpha 2-4 LOC-1M freeze-dryer and RZ-6 rotary vane pump (vacuum pump) used in this project. Photo: Cindy Zhang.* ***B)*** *depicts the single chamber system. Modified figure [56]. 18*

Figure 1.14*: Phase diagram of H_2O.* ***A)*** *Boiling point (100 °C) at atmospheric pressure (1013 mbar) where liquid and vapor form of H_2O can co-exist. At atmospheric pressure, increased temperature results in evaporation (liquid à vapor), and decreased temperature results in condensation (vapor à liquid). Red curve line shows a change in boiling point based on pressure.* ***B)*** *Melting/freezing point (0 °C) at atmospheric pressure where solid and liquid form of H_2O can co-exist. At atmospheric pressure, increased temperature results in melting (solid à liquid), and decreased temperature results in freezing (liquid à solid).* ***C)*** *The triple point (0 °C and 6.11 mbar) where solid, liquid and vapor form of H_2O can co-exist.* ***D)*** *For example, increased temperature above -40 °C (at 0.12 mbar) results in sublimation (solid à vapor), and decreased temperature below -40 °C (at 0.12 mbar) results in condensation (vapor à solid). Along the blue curve line indicates the values in which sublimation or condensation can take place. Modified figure [58]. 19*

Figure 1.15*: Examples of lyophilized drug product cake appearances.* ***A)*** *shows an example of total collapsed cake or meltback.* ***B)*** *shows no sign of collapse or cracking.* ***C)*** *shows an example of cracked cake. Photo: Cindy Zhang.....20*

Figure 1.16: *A vial containing a thermometer probe. The drying happens from the top and downwards with a sublimation front moving through the product, leaving a trail of dried product. Below the interface is the remaining frozen product to be sublimed. Self-drawn figure on Goodnotes 5.....21*

Figure 1.17: *Cryoprotectant's role in prevention of nanoparticle aggregation after reconstitution of lyophilized product. Created with BioRender.com with inspiration from [53]. 23*

Figure 4.1: *Sample content to produce nab-mitotane by DC. 31*

Figure 4.2: *The DC-step to produce nab-mitotane. Created with BioRender.com. 31*

Figure 4.3: *Incubation to induce the cross-linking process of the nanoparticles. Created with BioRender.com. ..33*

Figure 4.4: *The purification step by three cycles of differential centrifugation and redispersion. Created with BioRender.com. 34*

Figure 4.5: *The particle size analysis step, performed by PCS. Created with BioRender.com. 35*

Figure 4.6: *The sample preparation step. The weight of the vial and rubber stopper before and after adding the sample content were noted down. Created with BioRender.com. 37*

Figure 4.7: *The lyophilization-step starting with a freezing process before going over to the process of drying. After lyophilization, the samples are placed into the desiccator. Created with BioRender.com. 38*

Figure 4.8: *Preparing the samples for storage. The samples are either stored at room temperature or at refrigerated temperature. Created with BioRender.com. 38*

Figure 4.9: *The reconstitution and particle size analysis step. Created with BioRender.com. 39*

Figure 5.1: A) *Mean particle size and* ***B)*** *mean PDI of nab-mitotane obtained when using different amounts of ceramic beads (Ø: 0.3-0.4 mm) (mean ± SD, n = 4 (300 mg and 1200 mg) and 3 (750 mg)).....43*

Figure 5.2: A) *Mean particle size and* ***B)*** *PDI of nab-mitotane obtained based on the use of different sizes of ceramic beads and different amounts of ceramic beads (mean ± SD, n = 4 (Ø: 0.3-0.4 mm) and 2 (Ø: 1.4-1.6 mm)).* *44*

Figure 5.3: A) *Mean particle size and* ***B)*** *mean PDI of nab-mitotane obtained when different processing temperatures were applied during DC (mean ± SD, n = 3).* *47*

Figure 5.4*:* ***A) B)*** *Mean particle size and* ***C) D)*** *mean PDI of nab-mitotane obtained at different processing time during DC****. A)*** *and* ***C)*** *use BSA of pH 8.154-8.178, and* ***B)*** *and* ***D)*** *use BSA of pH 8.998-9.003 (mean ± SD, n = 3)..* *49*

Figure 5.5: A) *Mean particle size and* ***B)*** *mean PDI of nab-mitotane obtained when BSA solutions of different pH were used (mean ± SD, n = 3). pH 8 = 8.154-8.178; pH 9 = 8.998-9.003.* *50*

Figure 5.6: *Lyophilized cakes. Photos of the cake appearance of each sample were taken on day 0 and on the assigned day for reconstitution. n = 2. Photo: Cindy Zhang.* *53*

Figure 5.7: *Photos of cracked lyophilized cakes due to issues during the freezing process. Photo: Cindy Zhang.* *54*

Figure 5.8: A) *Mean particle size and* ***B)*** *mean PDI of nab-mitotane before and directly after lyophilization and reconstitution (mean ± SD, n = 2).* *55*

Figure 5.9: A) *Mean particle size and* ***B)*** *mean PDI of nab-mitotane, measured after lyophilization and reconstitution over a time period of 21 days and stored at room temperature (mean ± SD, n = 2).* *56*

Figure 5.10*:* ***A)*** *Mean particle size and* ***B)*** *mean PDI of nab-mitotane, measured after lyophilization and reconstitution over a time period of 21 days and stored at refrigerated temperature (mean ± SD, n = 2).* *57*

Figure 5.11: A) *Mean particle size and* ***B)*** *mean PDI of nab-mitotane, measured after lyophilization and reconstitution over a time period of 21 days and stored at room temperature (red bars) and refrigerated temperature (blue bars) (mean ± SD, n = 2). Results from storage at room temperature were individually compared to results from storage at refrigerated temperature at corresponding days.* *58*

List of abbreviations

ACC	Adrenocortical carcinoma
API	Active pharmaceutical ingredient
Approx.	Approximately
BCS	Biopharmaceutical classification system
BSA	Bovine serum albumin
cm	Centimeter
CYP	Cytochrome P450
DC	Dual centrifugation
e.g.	Exempli gratia / for example
EMEA	European Medicine Executive Agency
EPR	Enhanced permeability and retention
ER	Endoplasmic reticulum
FDA	Food and Drug Administration
G	gauge size (cannula)
gp60	60-kDa-gylcoprotein receptor,
h	Hour(s)
HSA	Human serum albumin
i.e.	Id est / that is / in other words
i.v.	intravenous
LDPE	Low density polyethylene
mbar	Millibar
M-EDP	Mitotane, etoposide, doxorubicin, and cisplatin
mg	Milligram
Min	Minute(s)
mL	Milliliter
mm	Millimeter
nab	Nanoparticle albumin-stabilized
ns	Not significant
o,p'-DDAC	o,p'-dichlorodiphenyl acylchloride
o,p'-DDD	1,1-dichloro-diphenyl-2,2-dichloroethane (mitotane)
o,p'-DDT	dichloro-diphenyl-trichloroethane
PCS	Photon correlation spectroscopy
PMMA	Poly(methyl methacrylate)
PP	Polypropylene

PPE	Personal protective equipment
RES	Reticuloendothelial system
rpm	Revolutions per minute
SD	Standard deviation
SOAT1	Sterol-O-acyl-tranferase 1
SPARC	secreted protein acid and rich in cysteine
T_c	Collapse temperature
TDM	Therapeutic drug monitoring
T_{eu}	Eutectic temperature
T_g	Glass transition temperature
T_p	Product temperature
Trp	Tryptophan
T_s	Shelf temperature
US or USA	United States of America
w/v	Weight per volume
g	Relative centrifuge force
Ø	Diameter
°C	Celsius degrees
µL	Microliter
µm	Micrometer
%	Percentage

1 Introduction

1.1 The role of mitotane in treatment of adrenocortical carcinoma

Mitotane has been used for the treatment of adrenocortical carcinoma (ACC) for several decades. It was first isolated in 1940, and the adrenolytic effect of Mitotane was observed through animal studies in dogs [1, 2]. In 1959 came the first clinical evidence in which the efficacy of mitotane for the treatment of ACC was reported in human patients [2, 3]. In 1970 in the United States, mitotane was approved for use in the chemotherapy of advanced ACC. Presently, it is commercially available in tablet form (500 mg) under the brand name Lysodren, administrated orally [4].

Clinical challenges are associated with the current treatment with mitotane. Orally administered, mitotane will have to be dissolved in the gastrointestinal tract to be able to be passively absorbed. However, mitotane is one of many active substances that are characterized as highly lipophilic, thus poorly soluble in water and resulting in low bioavailability [2, 5]. As mitotane is associated with unpredictable pharmacokinetics as well as having a narrow therapeutic window, the development of a new formulation is desired to increase the cytotoxic effects as well as reduce the therapy-limiting side effects. Injectable mitotane formulation is proposed, in which parenteral administration may alleviate some of the adverse effects and unpredictability associated with oral administration due to inter-individual variability. Additionally, parenteral administration could provide a better control of the mitotane plasma levels and potentially shorten the time it takes to reach the therapeutic levels [5].

So far, there are few publications that have addressed an intravenous (i.v.) application of mitotane. However, ever since the reported release of the successful nanoformulation with paclitaxel (marketed as Abraxane), the use of albumin as a nanocarrier for drug delivery has been a topic of interest. The binding of mitotane to albumin nanoparticles for an i.v. application could be a promising formulation strategy to circumvent the obstacles relating to the currently available application.

This project part-take in an ongoing formulation development study that use bovine serum albumin as a nanocarrier for mitotane. In this project, dual centrifugation (DC) was utilized in the preparation of albumin-stabilized mitotane nanoparticles. However, an issue in which this project will address to

is the yield of nanoparticles in sizes that are unfavorable for intravenous application (larger than 200 nm). Thus, a reduction of particle size is necessary to avoid immediate clearance due to opsonization in vivo [6]. The method by DC should therefore be optimized for obtaining smaller nanoparticles, in which will be the focus of this project. Further on, to get an idea about the stability of the albumin-stabilized mitotane nanoparticles in dried state, these nanoparticles will be lyophilized and undergo a short-term stability study.

1.1.1 What is adrenocortical carcinoma?

Adrenocortical carcinoma (ACC) is a rare form of adrenal gland tumor in which the malignant tumor cells form in the cortex of the adrenal glands (**Figure 1.1**) [7]. The incidence of ACC is 0.5-2 cases/million/year and can occur at any age [2, 8-10].

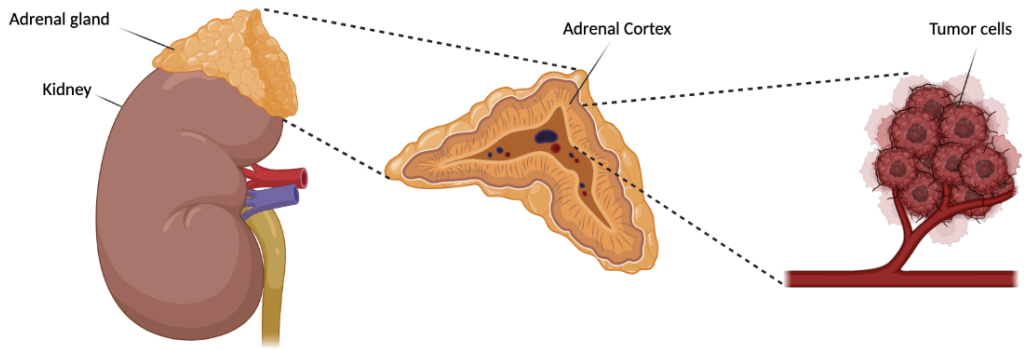

***Figure 1.1**: Adrenocortical carcinoma occurring in cortex of the adrenal glands. Created on BioRender.com.*

ACC can be divided in functional- or non-functional tumor. Functioning tumors can be found in up to 60% of the cases and can give rise to an excess of steroid hormones such as glucocorticoids, mineralocorticoids, and androgens. This can result in a manifestation of endocrine syndromes such as Cushing's syndrome (due to cortisone), virilization (due to androgens), feminization (due to estrogens) and hypertension (due to aldosterone). Patients with non-functioning tumors can present with symptoms such as back- or abdominal pain, nausea, and vomiting, with no abnormal increase in adrenal glands' hormone production [2, 7, 8, 11-14].

ACC is associated with poor prognosis and poor survival due to the rarity of the malignancy in addition to suboptimal medical treatment. The overall 5-year survival rate depends on varied factors. Prognosis is influenced by factors such as the tumor stage at the time of diagnosis, the overall condition of the patient, the possibility to remove the tumor completely, and if it is a functioning- or

non-functioning tumor [13, 15, 16]. If diagnosed early and in combination with complete surgical resection can lead to a 5-year survival rate of up to 81%. However, most cases are diagnosed at advanced stages that lead to a 5-year survival rate below 15%. Even after radical surgery, the recurrence rate remains high [13, 17-20].

Management of adrenocortical carcinoma

The only curative approach is complete surgical resection of tumor, whereas adjuvant treatments aim to reduce the risk of recurrence [11, 12]. For patients with localized ACC, surgical approach to perform complete resection of the tumor is the most effective therapeutic strategy [11, 12]. However, the odds for postoperative recurrence of the tumor are high. Most patients with ACC at earlier tumor stages would therefore benefit from adjuvant treatment (and possibly radiotherapy) after an evaluation of the risk of recurrence [11-13, 21]. The adjuvant treatment for ACC is referring to the use of the chemotherapeutic agent mitotane (**Section 1.1.2**). For patients that experience recurrent- or metastatic disease, mitotane therapy should be initiated as soon as possible [11, 12]. If mitotane monotherapy is inadequate, mitotane can be given in combination with another drug (such as streptozotocin) or polychemotherapy. Traditional cytostatic drugs such as etoposide, doxorubicin, and cisplatin in combination with mitotane (M-EDP) is recommended as first-line treatment in cases of rapid disease progression. Radiotherapy is another option that might be helpful for local recurrence in addition to medical therapy. [11-13, 21].

Mitotane plays an essential role in the treatment of ACC, but what is mitotane exactly?

1.1.2 What is mitotane?

Mitotane, 1,1-dichloro-diphenyl-2,2-dichloroethane (o,p'-DDD), is a compound that was isolated from the insecticide dichloro-diphenyl-trichloroethane (o,p'-DDT) [2, 13].

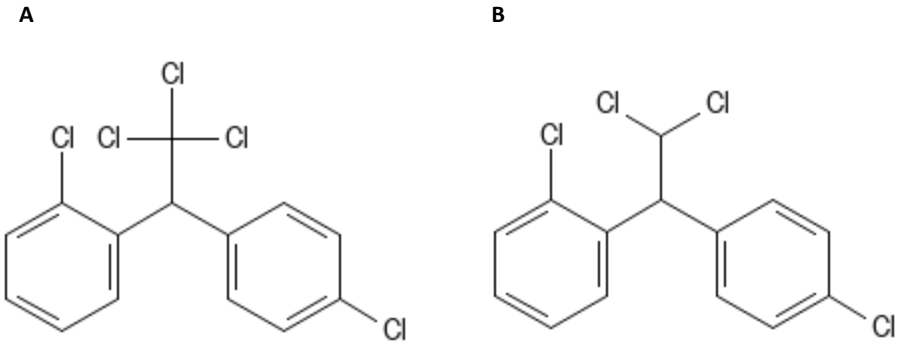

Figure 1.2: A) *The chemical structure of o,p'-DDT.* ***B)*** *The chemical structure o,p'-DDD, also commonly known as mitotane. Created on PubChem Sketcher V2.4.*

Mitotane is a highly lipophilic compound (**Figure 1.2B.**) with an experimental LogP and water-solubility at 6 and 0.1 mg/L (25°C), respectively [2, 5, 22]. It has shown to have antihormonal- and antitumoral activity, and is the only drug approved by the U.S. Food and Drug Administration (FDA) and European Medicine Executive Agency (EMEA) for palliative treatment of advanced ACC and for postoperative adjuvant therapy [4, 13, 19-21].

Pharmacological aspects of Mitotane

Mitotane has been used for the treatment of ACC for several decades. Presently, it is commercially available in tablet form (500 mg) under the brand name Lysodren, administrated orally [4].

Pharmacokinetic properties

Lysodren is administrated orally and should be taken during meals containing fat-rich food, which could improve the absorption of the active substance. The bioavailability through this administration route is considered low (up to 40%), possibly due to poor absorption and extensive metabolism. When absorbed, mitotane is distributed through binding to chylomicrons and lipoproteins and is thereafter primarily stored in fat tissues. Only free mitotane has shown to be therapeutically active. The half-life of mitotane elimination ranges from 18-159 days. The long elimination time is likely due to the accumulation of the drug in fat tissues because of its lipophilic characteristics, in which are

gradually redistributed in the plasma [1, 2, 23]. Metabolism of mitotane happens predominantly in adrenal cells. The drug can also be metabolized by cytochrome P450 (CYP) in the liver or intestine, thereby reducing its bioavailability. The most common CYP enzymes to be involved in mitotane metabolism is CYP3A4 and CYP2B6. Mitotane is known to be a strong inducer of CYP3A4, thereby accelerating its own metabolism (autoinduction) [5]

Pharmacodynamic properties

Mechanism of action

Currently, the mechanism of action of the drug is not yet fully understood.

Table 1.1 lists some of the mechanisms of action that have been reported through studies.

Table 1.1: *Examples of the mechanisms of action.*

Site	Effect of mitotane	Sources
Mitochondria in adrenocortical cells	▪ Interfering with the activation of steroidogenesis, thereby inhibiting the production of corticosteroids, and reducing the cell viability. ▪ Interfering with the respiratory chain complexes in which disrupts respiratory chain activity. This consequently inhibits the tumor cell proliferation and induces cellular apoptosis.	[1-3, 10, 13, 24]
Mitochondria-associated endoplasmic reticulum membranes (MAMs)	▪ Sterol-O-acyl-tranferase 1 (SOAT1) is located within MAM and are responsible for esterification of cholesterol. Inhibition of SOAT1 lead to accumulation of free cholesterol and other fatty acids inside the cells, which further caused lipid-induced endoplasmic reticulum (ER) stress, becoming toxic for the cells, triggering apoptosis.	[10, 13]

Clinical limitations

Mitotane has a narrow therapeutic index, leading to a requirement of therapeutic drug monitoring (TDM). To ensure both therapeutic efficacy as well as avoiding increased toxicity as much as possible, the targeted blood levels of mitotane is a plasma concentration between 14-20 mg/L [12, 13, 23, 25, 26]. The inability to predict the plasma concentrations of mitotane due to high distribution volume and the long half-life of the drug (18-159 days), as well as individual differences and to avoid toxic levels, it usually takes a long time to be able to attain the therapeutic plasma concentrations of mitotane. To reach the targeted plasma concentrations usually takes several months, normally

around 3-5 months. Side effects such as adrenal insufficiency, dizziness, nausea, vomiting, and diarrhea are very common which often makes it difficult to reach the targeted blood levels due to limited tolerability [3, 5, 23, 25, 26]. Plasma levels exceeding 20 mg/L may be associated with severe adverse effects and have not been shown to improve efficacy [25].

The prolonged time to reach the targeted plasma concentrations limits the clinical utility of the drug. It causes a delay in tumor treatment and can give rise to drug toxicity [23]. To ensure optimal use of mitotane, the dosing should be individually adjusted by monitoring the blood levels as well as the clinical tolerance of the drug, until the therapeutic range is reached [25]. This way, it could lead to more anticipated and rapid attainment of the therapeutic levels which further could potentially improve the clinical management of the treatment. Moreover, it is important to maintain adherence to the treatment and to help the patients deal with the side effects. It is therefore important to establish a close relationship between the patient and the physician to ensure compliance [25].

Due to these limitations that arise from the current formulation on the market, development of new formulation for mitotane is desired.

1.2 Formulation development for mitotane

The toxic side effects that arise during the treatment with mitotane can limit tolerability and urge the discontinuation of treatment [2, 5]. Thus, formulation development that can both improve efficacy as well as decrease toxicity is desirable. Due to the unfavorable pharmacokinetic profile of mitotane possibly attributed to the oral application, an alternative dosage form could be beneficial. Nanotechnology and the development of nanoformulations have gained prominence in recent years to tackle the poor water solubility issue associated with most APIs. Therefore, this section will further present nanoformulation as a possible option for a dosage form.

1.2.1 Nanoformulation as a potential formulation for parenteral administration

Nanotechnology and nanoparticle systems

Nanotechnology offers possibilities for developing new pharmaceutical dosage forms and drug delivery systems, utilizing the unique physicochemical properties in the nano dimension to explore

for new application. Nanoparticle-based systems can be classified as nano-sized active drug particles, or as nano-sized substrates that can encapsulate active pharmaceutical ingredients (APIs) within [27]. The size of a nanoparticle can vary depending on the intended application, but some might argue a general range can be considered between 100-500 nm or even up to 1000 nm [28]. However, the lower size limit is often reported to be 1 nm. The other end of the scale is often harder to define as there is no universally accepted definition. In nanomedical applications, the preferential size is less than 200 nm. Nanoparticles larger than 200 nm will activate the complement system, and thus be quickly removed from the blood steam and accumulated in the liver and spleen [28, 29]. Nevertheless, the upper limit is more commonly reported to be approx. 100 nm [30]. According to the U.S. FDA, a nanoparticle's dimension is 1-100 nm [27, 31].

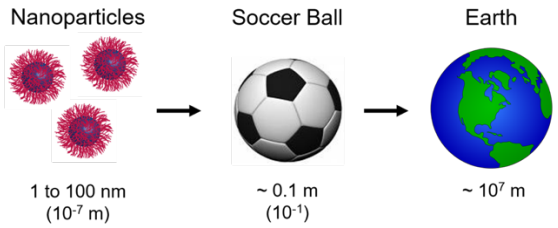

Figure 1.3: *Size comparison between a nanoparticle, a soccer ball and planet earth. The difference in size between a nanoparticle and a soccer ball is the same as the difference in size between the soccer ball and earth [32].*

In nanomedicine, nanoparticles are not only able to enhance the water solubility of lipophilic APIs but are also engineered as delivery vehicles for therapeutics (or imaging agents, or both) with an aim to improve clinical outcomes. However, it is necessary to design the nanoparticles so that they can be efficiently delivered to the diseased site of the body (such as the tumor site), and preferably in a controlled manner [33].

For the treatment of ACC, a few researchers have attempted to optimize the mitotane formulation, but with a limited success rate [5]. The development of formulation downsized into the nanometer-range can be of potential, as nanopharmaceuticals can overcome some of the limitations of conventional medicines by promoting both improved pharmacokinetics and pharmacodynamics, independent of the molecular structure of the active substance [31]. Some examples of carriers that can be utilized in nanoformulations can be seen in **Figure 1.4**. However, these nanoformulations need to undergo preclinical and clinical studies to characterize the pharmacokinetics and -dynamics, biodistribution, efficacy, and toxicity to understand how they differ from e.g. the conventional dosage forms, as nanoparticles can alter the pharmacokinetics considerably [31].

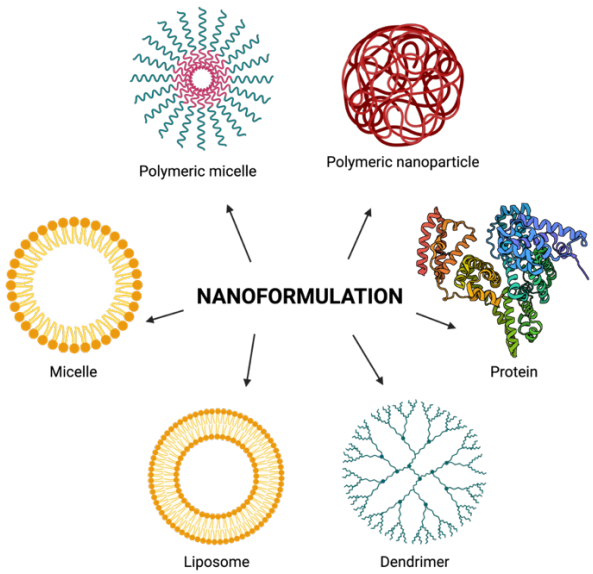

Figure 1.4: *Examples of various types of nanocarrier systems. Created with BioRender.com.*

Due to the small sizes of the nanoparticles, they are able to pass through biological barriers. Additionally, they can be designed to detect, target, and accumulate in tumors for cancer treatment through passive- or active targeting [34]. Thus, nanoparticles can be beneficial through improved solubility and pharmacokinetics, enhanced efficacy, and reduced toxicity by allowing targeted cancer therapy and/or by minimizing the accumulation in healthy tissues [31, 34]. **Figure 1.5** shows an example of a drug delivery vehicle with targeting capabilities.

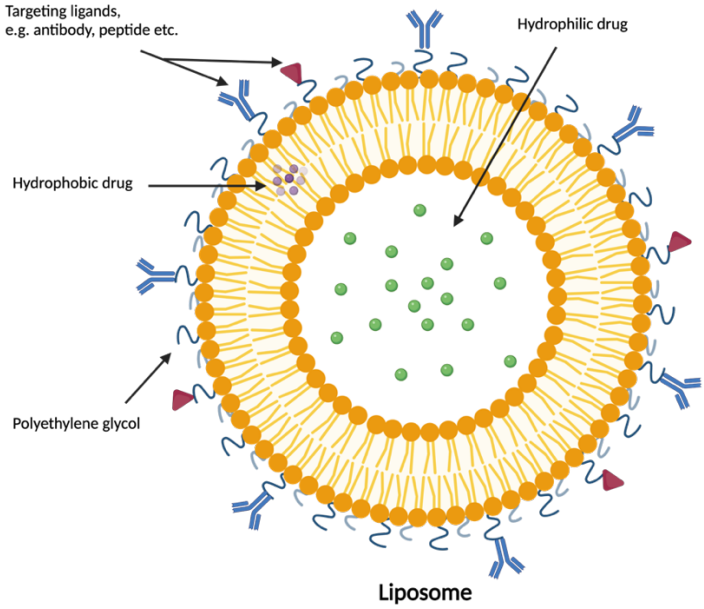

Figure 1.5: *A schematic representation of a targeted liposomal drug delivery system. Created with BioRender.com.*

Targeting can enable higher levels at the targeted site, therefore lower doses might be needed to achieve therapeutic efficacy. Furthermore, the reduction of the dose required to achieve therapeutic effect can result in reduced adverse effects (thereby improving patient tolerability) in addition to decreased treatment costs [31]. On the other hand, elevated levels of active substance at the targeted tumor site instead of healthy tissues might allow better tolerance for higher doses. This way, an increased cytotoxic effect can be transpired without a concomitant increase in side effects [35].

In short, applying nanotechnology for medicinal purposes can offer many advantages. As many of the core problems are directly correlated to the physicochemical properties of mitotane and its current route of administration [5], an injectable dosage form utilizing nanocarrier systems can be the solution to circumvent these drawbacks. Potential advantages related to an injectable nanoformulation are summarized in **Figure 1.6**, including the possibility of tumor targeting.

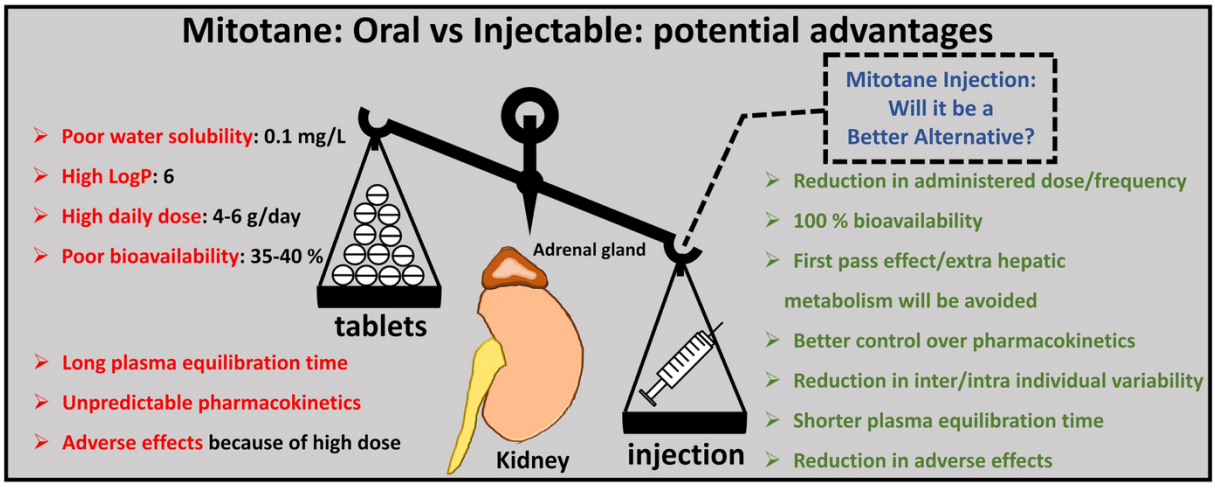

Figure 1.6: *A summary of potential advantages with an injectable dosage form in comparison to an oral dosage form [5].*

To the best of the author's knowledge, there are few publications that have addressed an i.v. application of mitotane. However, ever since the reported release of Abraxane, a nanoformulation with paclitaxel, the use of albumin as a nanocarrier for drug delivery has been a topic of interest.

Utilizing albumin as a nanocarrier for drug delivery

Nanoparticle-based systems have been demonstrated to be promising strategies in active- or passive targeting, in addition to prolonged blood circulation time. An example of a nanoparticle-based system is the use of albumin as a nanocarrier. Albumin is a component of the human blood as an

endogenous protein and has been widely used as a clinical excipient in many formulations [35]. Abraxane, an albumin-stabilized form of paclitaxel indicated for metastatic breast cancer [36], is a well-known case.

The potential of albumin-based nanocarrier

Nanoparticles made of albumin can offer several advantages as summarized in **Figure 1.7**. First of all, albumin is a component of the human blood. It is a natural carrier of hydrophobic molecules such as vitamins and hormones, to be delivered to target tissues [37, 38]. Additionally, as an endogenous protein, it has shown to be non-toxic, biodegradable, biocompatible, non-immunogenic, highly water-soluble, and a stable plasma protein, making it an ideal candidate for drug delivery [35, 39]. Moreover, albumin has a relatively long half-life (19 days) which can help maintain a high plasma concentration of a drug over a relatively long period of time [35]. Also, it has been reported that albumin can act as an excellent lyoprotectant. This allows the solid formulation of nanopharmaceuticals and immediate redispersion of dried nanoparticles into injectable solutions [35, 40]. Another advantage is that albumin, in cancer therapeutics, can provide tumor specificity (**Figure 1.8C**)[41].

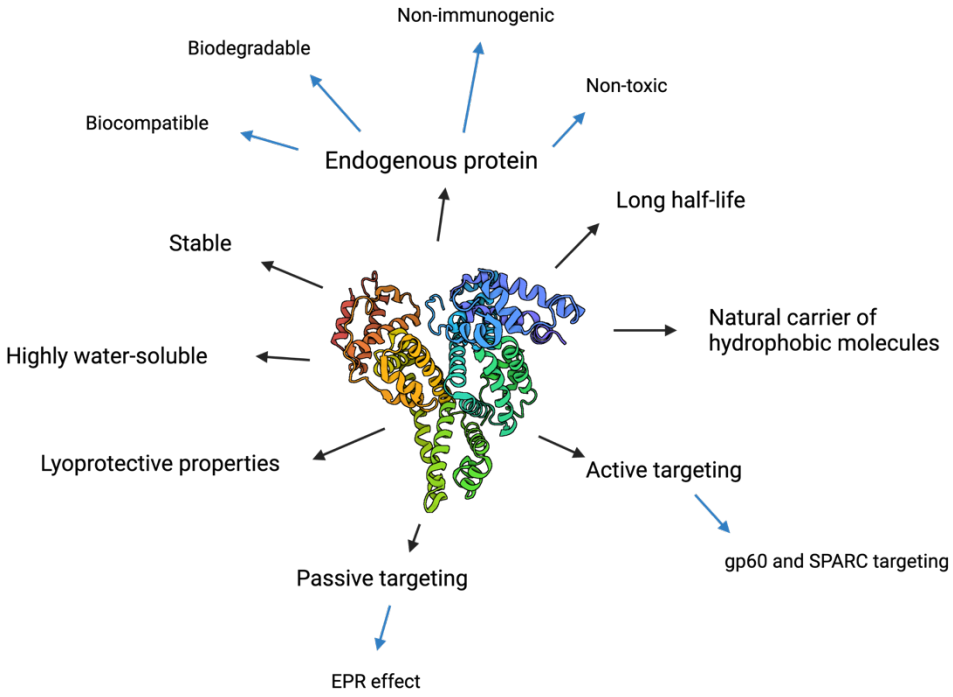

Figure 1.7: *Advantages of albumin-based nanoparticles. Created with BioRender.com.*

Albumin has been shown to be successfully applied as a nanocarrier in nanomedicine. As recently mentioned, Abraxane is a well-known example, introducing nanoparticle albumin-stabilized paclitaxel (nab-paclitaxel) in treatment for metastatic breast cancer, advanced pancreatic cancer and as combination therapy for non-small lung cancer [38]. In comparison with Taxol (a formulation of free paclitaxel) which is highly dependent on solvents in order to dissolve the highly water-insoluble active substance, nab-paclitaxel has demonstrated how a traditional cytostatic drug could achieve enhanced therapeutic results through improved drug delivery and pharmacokinetics with nab-technology [37, 38, 42].

Due to the water-soluble character of albumin, it can enhance the aqueous solubility of the otherwise lipophilic drug. The long half-life of albumin can provide improved pharmacokinetic profile of the drug, in addition to increasing tumor accumulation of the drug as albumin has shown a preferential uptake in tumors through passive targeting [42, 43]. Due to the leaky blood vessels combined with impaired or lack of lymphatic drainage system in the malignant tumor tissues, albumin among other macromolecules can accumulate at the solid tumor site through the enhanced permeability and retention (EPR) effect (**Figure 1.8B**). In contrast, healthy tissues only allow small molecules to pass through the endothelial barrier (**Figure 1.8A**) [42]. It is possible to further improve tumor targeting by modification of targeting ligands on the surface of the albumin-based nanoparticles, providing active targeting. Moreover, a systematic review on the use of albumin in nanomedicine showed alleviation of in vivo side effects and drug toxicity, which could provide the possibility of higher doses to be administrated that could potentially increase the efficacy with no elevation of side effects [35]. Thus, albumin could be utilized in cancer therapy. The enhanced uptake of albumin-based nanoparticles is also due to transcytosis across the vascular endothelium [39, 42]. Active internalization of albumin in tumors is initiated by the binding of albumin to 60-kDa-gylcoprotein (gp60) receptor and SPARC (secreted protein acid and rich in cysteine), which is briefly demonstrated in **Figure 1.8**C.

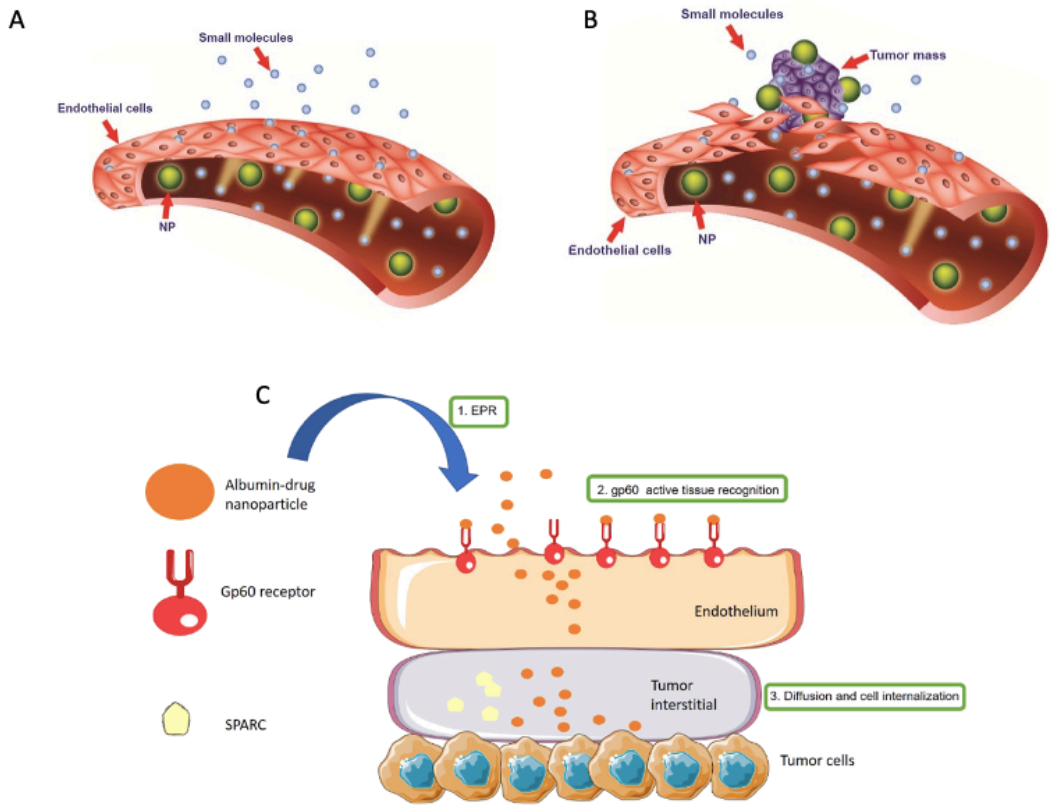

Figure 1.8: *A) Normal blood vessel. B) Leaky blood vessel at tumor site. C) Accumulation of albumin-stabilized drug nanoparticle at tumor site through transcytosis [44, 45].*

There are commonly two types of albumins that are used when constructing nanoparticles: human serum albumin (HSA), and bovine serum albumin (BSA) [35]. The two types share a lot of similar properties, such as high water-solubility, long half-life, and similar molecular weight and number of amino acids residues [35]. Their structures can be seen in **Figure 1.9.**

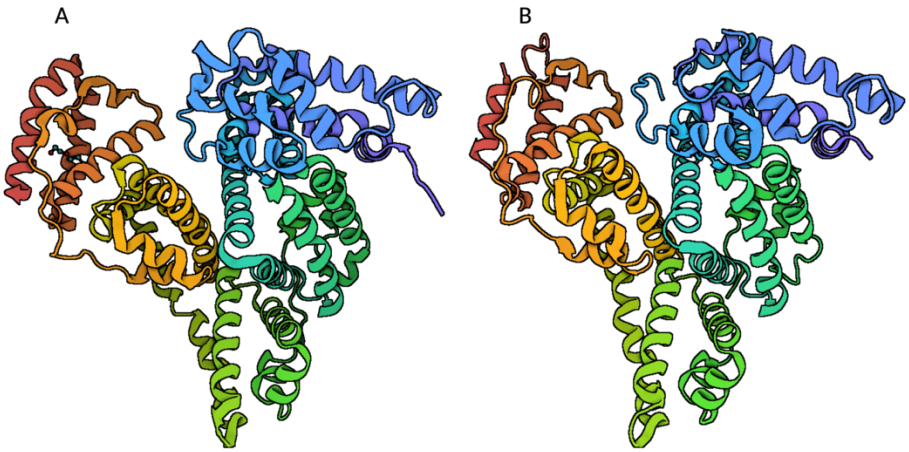

Figure 1.9: *Structures of **A)** BSA and of **B)** HSA. Created with BioRender.com, PDB ID 4F5S (BSA) and 7DJN (HSA).*

Bovine serum albumin vs. human serum albumin

Bovine serum albumin (BSA) has a molecular weight of 69.3 Da and consists of 583 amino acid residues. It is a carrier of interest for drug delivery due to its abundance, low cost, ease of purification, and its similarity to human serum albumin (HSA), making it less immunogenic compared to albumin from egg white and rat serum. Moreover, it has a widespread acceptance in the pharmaceutical industry with a good ability to bind to a wide variety of both endogenous and exogenous compounds [41, 46].

On the other hand, HSA have a molecular weight of 66.5 Da and consists of 585 amino acid residues. Due to the presence of more acidic amino acids compared to basic amino acids, HSA contain a negative charge. The disulfide bridges provide stability, exhibiting a biological half-life of 19 days on average. It is also extremely robust towards factors such as pH, showing stability in the pH range of 4-9; temperature, showing an ability to endure heat up to 60 degrees for 10 hours without being damaged; and organic solvents [39, 41, 42, 46].

BSA and HSA share 76% sequential identity. The biggest difference between the two albumins is regarding the positions and numbers of tryptophan (Trp) residues. While HSA only has one Trp, BSA has an additional one [41]. Both kinds of albumin have been widely used to produce nanoparticles in nanomedicine [35]. Although compared to other albumins, HSA is more non-immunogenic and is widely used as a safe and effective carrier protein in different delivery systems [41].

Utilizing albumin as a nanocarrier for mitotane for i.v. application could be a promising formulation strategy to circumvent the mentioned clinical challenges associated with the current existing formulation. However, one of the biggest challenges in general regard to drug delivery systems is targeted drug delivery, controlling drug release, and preventing opsonization [47].

This project part-take in an ongoing formulation development study that use BSA as a nanocarrier for mitotane. There are several different techniques in which nanoparticles can be produced. For example, desolvation is a common method to obtain nanoparticles. To produce albumin nanoparticles, a desolving agent such as ethanol is dropwise added into an aqueous solution of albumin under constant stirring until turbidity is observed. Additionally, a cross-linking agent such as glutaraldehyde is added in order to stabilize the resulted nanoparticles. However, a drawback with this technique was a low drug-loading in the case of mitotane [unpublished data]. Another well-established method to produce albumin-based nanoparticles of the drug is through high-pressure

homogenization. The drug and albumin are mixed in an aqueous solvent, and thereafter passed through a narrow channel under high pressure [39]. The issue with this method is the possibility of contaminating the sample material with residues from the homogenizer, as the samples are in direct contact with the unit . Thus, another method to produce nanoparticles of albumin and the drug were needed. In this project, dual centrifugation (DC) was utilized in the preparation of albumin-stabilized mitotane nanoparticles, or so-called “nab-mitotane” in which this thesis will further address the formulation.

1.3 Dual centrifugation as a method to produce nanoparticles

DC is a homogenization tool that allows the use of closed and disposable vials, in addition to the preparation of small sample sizes. This method provides several advantages. Being able to use closed and disposable vials makes it possible to avoid contamination of the samples as well as the need to clean the DC device. This is especially of importance when handling cytostatic substances such as mitotane. Preparation of small sample sizes is also beneficial when only small amounts are needed and when the raw materials are expensive or rare. Additionally, this apparatus allows the process of more than one sample at a time, enabling samples of differences in composition to be run simultaneously for comparison [48]. This method can therefore provide time- as well as cost-effectiveness.

1.3.1 Principles of dual centrifugation

Whilst DC is based on centrifugation, it differs from normal centrifugation by having an additional, secondary rotation of the samples (**Figure 1.10**). Meaning, in addition to turning around a main, central axis, the samples have a second rotation axis which ensures that the high centrifugal acceleration in the sample vials changes direction fast and continuously. Thus, in comparison to normal centrifugation, DC is not a separation technique, but rather a technique used for e.g., powerful sample mixing, milling, and homogenization. Due to the fast change of direction of the centrifugal acceleration within the sample vial, it creates powerful movements of the samples that contribute to effective homogenization or milling [48, 49].

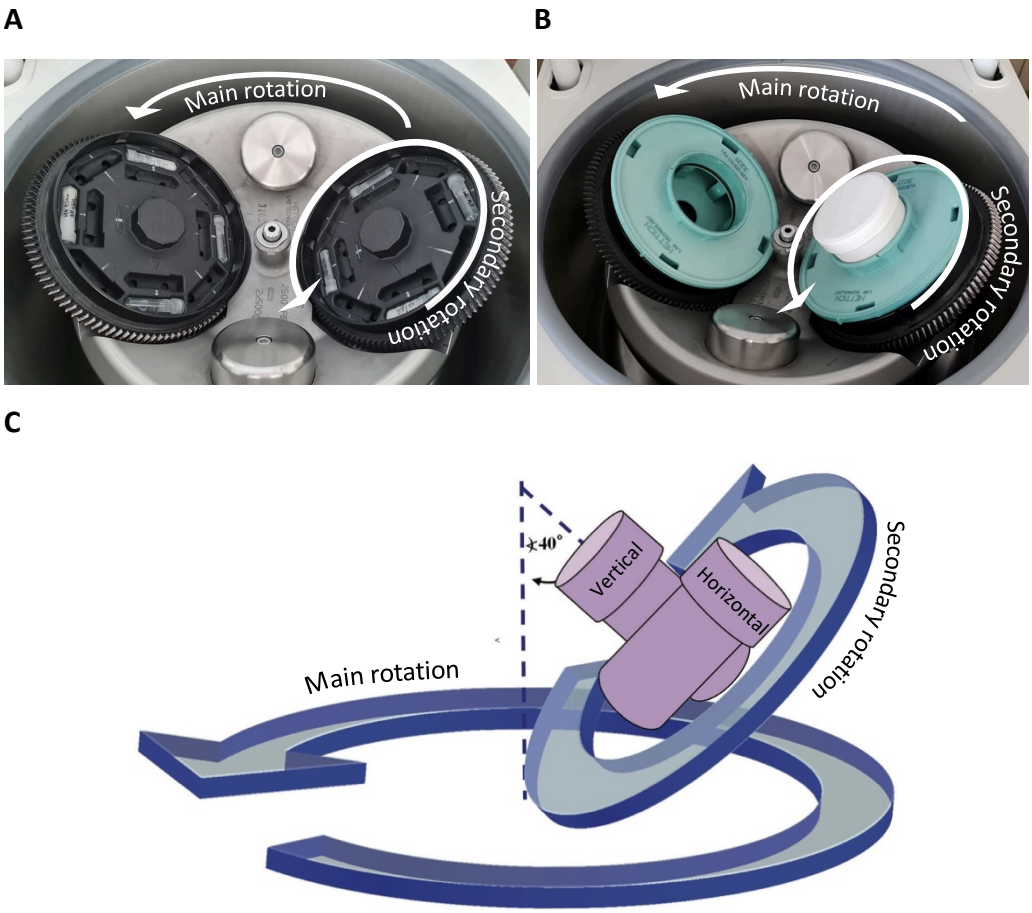

Figure 1.10: A) *The set-up of dual centrifuge ZentriMix 380 R with a major (main) rotation and sample (secondary) rotation. The sample vials are placed into the secondary dual rotor in horizontal orientation. Photo: Cindy Zhang.* ***B)*** *Set-up with sample vials placed into the secondary dual rotor in vertical orientation. Photo: Cindy Zhang.* ***C)*** *Schematic view of vertical and horizontal vial orientation. Modified from [48].*

Several factors can influence the homogenization power of the DC, such as rotating speed around the main and secondary axis in addition to the shape and the orientation of the sample vial. The rotating speed determines the centrifugal acceleration and the frequency of the change of direction of centrifugal acceleration within the sample vial. Moreover, the shape and orientation of the sample vial placed inside the dual rotor will have a strong influence on the homogenization power due to the distance within the vial in which the sample material will be transported. The horizontal vial orientation is as depicted in **Figure 1.10A**, placed into the secondary dual rotor in a way that ensures that the centrifugal acceleration changes continuously while turning around the second axis. Using a lengthy sample vial, the sample material will gain speed and kinetic energy to move across the vial, being able to clash to the top or the bottom of the vial with high impact during the rotations. This is especially efficient when the sample material is to be homogenized in small vials. The alternative vial

orientation, however (**Figure 1.10B**), is placed vertically into the center of the secondary dual rotor, where the movements of the sample material result in strong fiction and shear forces, this way ensuring homogenization. This is especially efficient when using vials with large diameters [48].

Another factor that can affect homogenization and milling is the use of homogenization aids. Adding homogenization aids such as heavy beads (e.g., glass- or ceramic beads are common material of choice) will stir the sample material into rapid motion. Whilst the two rotations introduce high-stress intensities in the samples, they can be further increased by using these grinding aids. Additionally, the beads create bead-bead interactions by moving through the sample material in order to collide with each other, thus improving the homogenization [48]. This is also critical for the particle size of the sample material, which has been demonstrated to efficiently reduce the particle size [50]. For this project, ceramic beads are used as homogenization aid. These beads are made of yttria-stabilized zirconia, and are on a higher scale in terms of density and hardness compared to glass beads [48].

DC parameters such as processing time might also affect the degree of homogenization to a certain extent due to the stress induced inside the sample vials, thus affecting the resulting size of the produced nanoparticles [48]. In addition to processing temperature, the influence of these two parameters on the size of nab-mitotane will be further investigated.

Further on, to get an idea of the extension in which the stability of nab-mitotane is preserved in dried state, these nanoparticles will be lyophilized. To the best of the author's knowledge, there has been no reports regarding a stability study of lyophilized nab-mitotane. Thus, a first lyophilization study is conducted. An introduction to the general principle of lyophilization is further on presented in the next sections.

1.4 Lyophilization for improved stability

In the development of pharmaceutical drug products, it is desirable with an extended shelf-life of the drug product. One important challenge in the development of nanoparticles is their long-term stability upon storage [51].

Aqueous dispersions are known for being microbiologically-, physically-, and chemically unstable. The presence of water creates a suitable environment for microbiological growth, in which can result in

biological deterioration of e.g. proteins [52]. Simultaneously, sedimentation and fusion of nanoparticles such as aggregation and agglomeration can occur over time, which is roughly demonstrated in **Figure 1.11** [53].

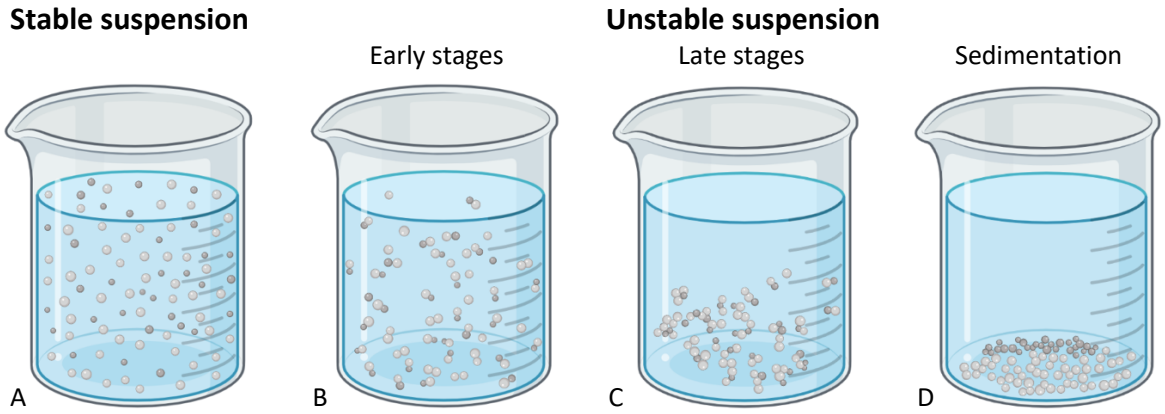

***Figure 1.11**: **A)** stable suspension – a uniform dispersion of particles. **B-D)** unstable suspensions – aggregation and agglomeration in which particles stick to each other, likely followed by sedimentation. Created with BioRender.com*

On the other hand, chemical instability includes undesirable chemical reactions that can take place during long-term storage. The main chemical reactions that can affect the stability of drugs or drug formulations are hydrolysis and oxidation. Deamidation is also a common degradation route in proteins [52, 54]. Oxidation reactions can often be reduced to acceptable levels by storing the drug products in the absence of light or oxygen. Hydrolysis (and deamidation for proteins) are however a more common issue. Upon exposure to humidity, the presence of water can initiate cleavage of bonds within the molecules. Such degradation can lead to loss of potency or efficacy [54]. Thus, removal of water can effectively prevent these deteriorations and can allow a more convenient storage of the products, such as stability for long-term storage at ambient temperatures [55]. Freeze-drying is a commonly used process to enable long-term stability of pharmaceutical formulations [51, 53, 54]. Formulations in form of e.g., solutions, emulsions, colloids, or suspensions with limited stability may be stored in lyophilized, dried state. The freeze-dryer used in this project is shown in **Figure 1.12**.

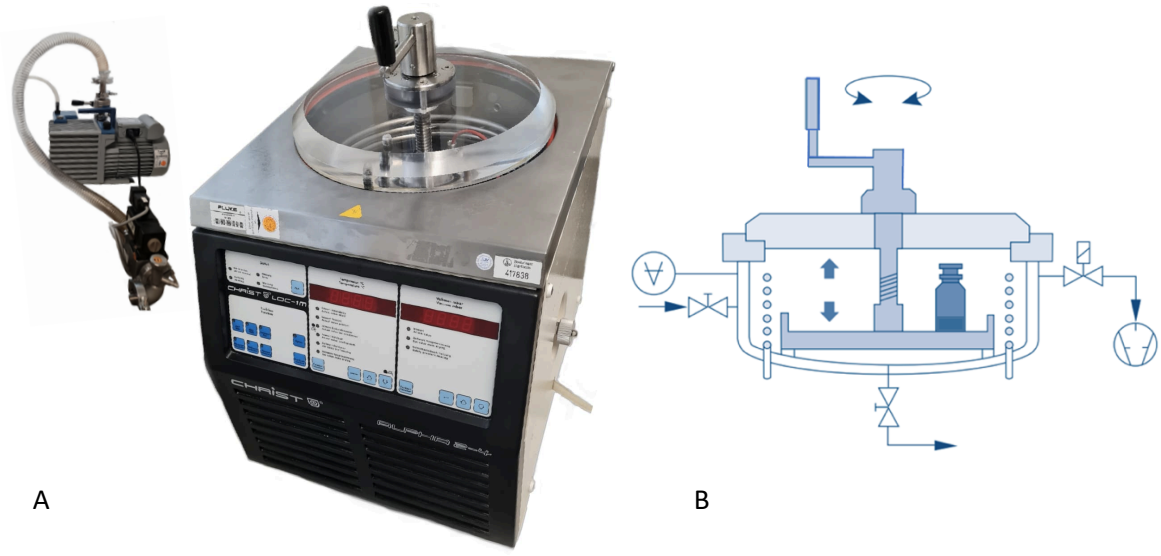

A B

Figure 1.12: A) *Christ® Alpha 2-4 LOC-1M freeze-dryer and RZ-6 rotary vane pump (vacuum pump) used in this project. Photo: Cindy Zhang.* ***B)*** *depicts the single chamber system. Modified figure [56].*

1.4.1 Principle of lyophilization

Lyophilization, also known as freeze-drying, is an effective way of drying materials without causing excessive damages due to high-temperature treatments. It is a process of choice in the pharmaceutical industry, allowing stability and thus extended shelf-life of both small molecular therapeutics and biopharmaceuticals that are heat-sensitive [57]. It can be particularly suitable for biomolecules such as proteins. This process involves the removal of water from a frozen solution by sublimation under vacuum with gentle heating (primary drying). This is followed by a secondary drying, involving further heating to more elevated temperatures to remove the residual bound water molecules [52]. Sublimation involves the direct transition between solid state (ice) and the gaseous state (vapor) without passing though the liquid phase (water). To achieve this, the frozen product is dried under vacuum while avoiding the process of melting [56].

The basic principle of sublimation can be explained with reference to a phase diagram for the water system. In a graph with pressure (mbar) as a function of temperature (°C), the diagram consists of three separate areas that represents the different phases of water: vapor, liquid and solid (**Figure 1.13**). Along the lines on the graph, two phases can coexist under the condition of temperature and pressure that is defined by the line. However, there is a unique point at approx. 0 °C and 6.11 mbar that allows all three phases of water to coexist, called the triple point. With a pressure less than 6.11 mbar, H_2O can pass directly from the solid to the gaseous state and vice versa. Sublimation occurs when solid ice is maintained at pressure below the triple point and upon heating [56, 57].

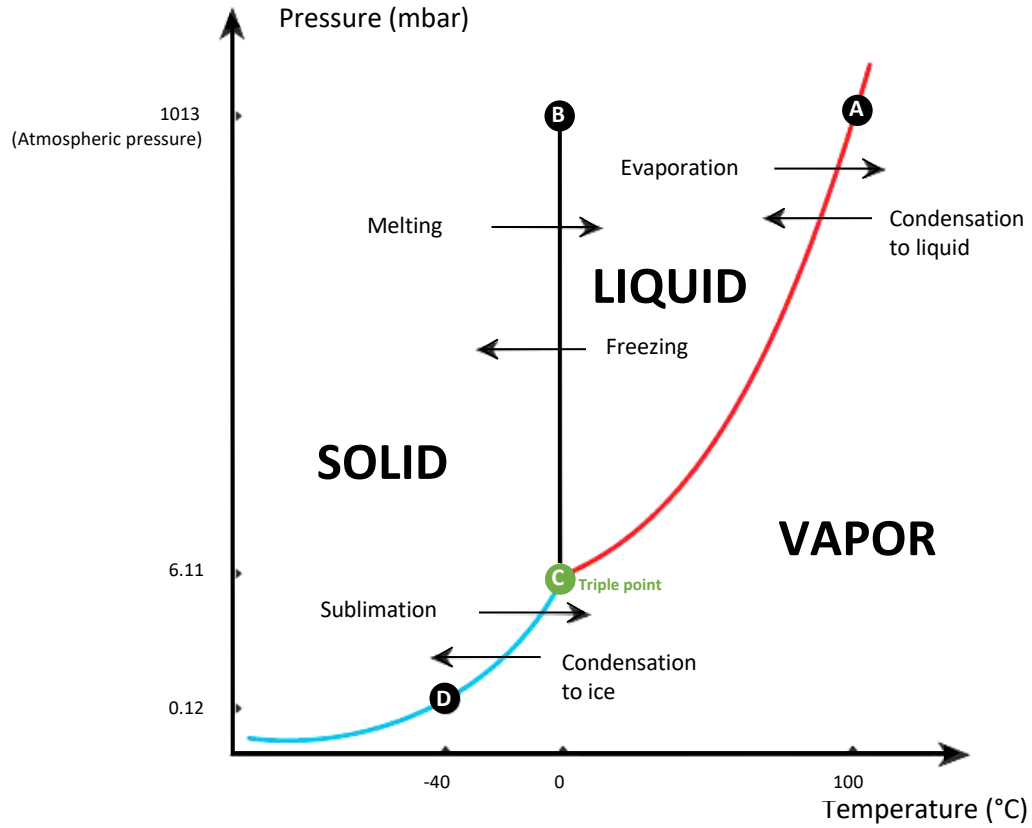

***Figure 1.13**: Phase diagram of H_2O. **A)** Boiling point (100 °C) at atmospheric pressure (1013 mbar) where liquid and vapor form of H_2O can co-exist. At atmospheric pressure, increased temperature results in evaporation (liquid à vapor), and decreased temperature results in condensation (vapor à liquid). Red curve line shows a change in boiling point based on pressure. **B)** Melting/freezing point (0 °C) at atmospheric pressure where solid and liquid form of H_2O can co-exist. At atmospheric pressure, increased temperature results in melting (solid à liquid), and decreased temperature results in freezing (liquid à solid). **C)** The triple point (0 °C and 6.11 mbar) where solid, liquid and vapor form of H_2O can co-exist. **D)** For example, increased temperature above -40 °C (at 0.12 mbar) results in sublimation (solid à vapor), and decreased temperature below -40 °C (at 0.12 mbar) results in condensation (vapor à solid). Along the blue curve line indicates the values in which sublimation or condensation can take place. Modified figure [58].*

Stages of freeze-drying process

Freezing stage

The freezing or solidification step is critical, which determines the morphology of the frozen material that influence the final freeze-dried product. During the freezing step, the sample is frozen under atmospheric pressure, before the application of a vacuum to avoid frothing [57]. As the process proceeds, the viscosity of product increases and water is converted to ice crystals. An amorphous, crystalline, or combined amorphous-crystalline solid will be obtained, in which the morphology of the frozen material will have influence over primary- and secondary drying such as the sublimation rate [53, 57, 59].

Due to the presence of dissolved solutes in the aqueous solution, the sample must be cooled to well below the freezing temperature for water. The necessary temperature to complete the solidification of the formulation will depend on the nature of the solvent, drug, and excipients. It is important to consider the critical formulation properties during the freezing stage, such as the glass transition temperature (T_g), eutectic temperature (T_{eu}) and the collapse temperature (T_c). T_c is usually 1-3 °C higher than the T_g values for amorphous materials or T_{eu} if solutes are crystallized in frozen solution. Drying above the T_c may result in collapse of the lyophilizate, as shown in **Figure 1.14A** [60-62]. The temperature is set by adjusting the shelf temperature (T_s) to below T_g or T_{eu}, and kept at that temperature long enough for all the solution to become solid [60]. In order to produce an acceptable freeze-dried product, it is always required to freeze-dry a formulation at the temperature lower than T_c [62].

Primary drying

The sublimation take place under the drying stage. Applying chamber pressure is an important parameter as it affects both heat and mass transfer. It allows the primary drying to be carried out at low pressure, which can improve the rate of ice sublimation. The freeze-dryer must be connected to a source of a vacuum that can sufficiently reduce the pressure below the triple point (an example shown in **Figure 1.12**). Simultaneously, the vapor formed during the drying must be removed. In this stage, some heat is applied to initiate the sublimation of ice crystals that were formed during the freezing stage. As the sublimation process proceeds, the frozen mass changes into a cake-like structure (**Figure 1.14B**) [60]. Most of the moisture is removed during the primary drying stage.

Figure 1.14*: Examples of lyophilized drug product cake appearances.* ***A)*** *shows an example of total collapsed cake or meltback.* ***B)*** *shows no sign of collapse or cracking.* ***C)*** *shows an example of cracked cake. Photo: Cindy Zhang.*

The T_s is also an important parameter as it affects the rate of drying. It controls the product temperature (T_p) by constantly transferring heat or providing the necessary energy for sublimation. However, T_p should always remain several degrees below T_c to obtain a freeze-dried product with

acceptable appearance. T_p can be monitored by methods such as using temperature sensor such as thermocouples (as shown in **Figure 1.15**) [60, 62].

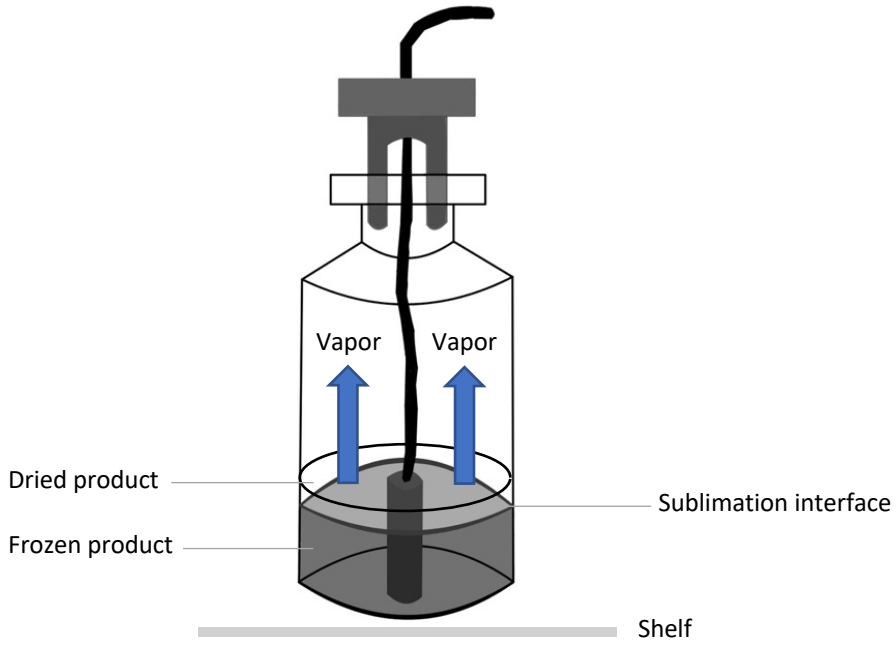

Figure 1.15: *A vial containing a thermometer probe. The drying happens from the top and downwards with a sublimation front moving through the product, leaving a trail of dried product. Below the interface is the remaining frozen product to be sublimed. Self-drawn figure on Goodnotes 5.*

Determination of the end point of the primary drying can be done by several different methods. The most basic is by monitoring the T_p with a thermocouple probe. During this stage, most of the water is removed. When there is no ice present in the vials, the T_p will increase and approach the T_s. Graphically, the T_p as a function of time will show a rise in temperature over time, followed by a plateau when T_s is approached and thus indicating the end point of primary drying. However, by using a thermocouple to monitor the temperature in the vials can be misleading, as the vial with the thermocouple can not be representative for the whole batch. That vial will have different freezing- and heating behavior, as the thermocouple can for example conduct more heat [62, 63]. This can result in faster drying for that specific vial. Therefore, it is important to allow additional amount of drying time to ensure that the ice in the entire batch is completely sublimed. Due to the product drying from the top and downwards, the thermocouple should be placed in the center of the vial, and at the bottom as shown in **Figure 1.15** [63].

Secondary drying

Whilst the ice has been sublimed during the primary drying, there are still a fair amount of residual moisture (up to 5-20%) that did not sublime off at the end of that stage. That is water molecules that are sorbed to the product. The objective of secondary drying is to reduce this residual moisture content to levels that results in optimal stability, usually less than 1% [52, 62, 63]. Desorption of the water molecules can happen by raising the T_s. Due to the absence of ice after the primary drying, high temperatures may be applied without the fear of melting or collapse as the small amount of residual moisture is not sufficient to cause spoilage [57]. The T_s in secondary drying is much higher than the temperature applied during primary drying so that desorption of water can occur at more practical rate [62].

Addition of cryo- and lyoprotectant

Freezing and dehydration can generate stresses due to the shock caused by the low temperatures, osmotic shrinkage and rehydration [53]. This can compromise the stability of colloidal suspension of nanoparticles. During the freezing stage of the sample there is a phase separation, one of which is ice and the other of nanoparticles and other components such as buffers and unloaded drugs. This separation can induce fusion of nanoparticles. Additionally, the formation of ice crystals may exercise a mechanical stress on the nanoparticles, leading to their destabilization [53, 64]. In order to prevent the stresses caused during the freezing and drying stages, special excipients can be included in the nanoparticle formulation before starting the lyophilization process. These excipients are inert substances that can be added to a pharmaceutical product to improve the stability both during the lyophilization and storage. These are typically divided into two categories: cryoprotectant and lyoprotectant. Cryoprotective agents are added to protect the product from stress during the freezing stage, while lyoprotective agents work to prevent stresses caused during the drying stages [53]. **Figure 1.16** demonstrates how cryoprotectants work to prevent nanoparticles aggregation after reconstitution of lyophilized product. Cryoprotectants can serve as stabilizers. A theory about how these agents can stabilize nanoparticulate systems are through a mechanism called “water replacement”. These stabilizers can form hydrogen bonds on the surface of the nanoparticles, substituting for the water lost during the drying process [51].

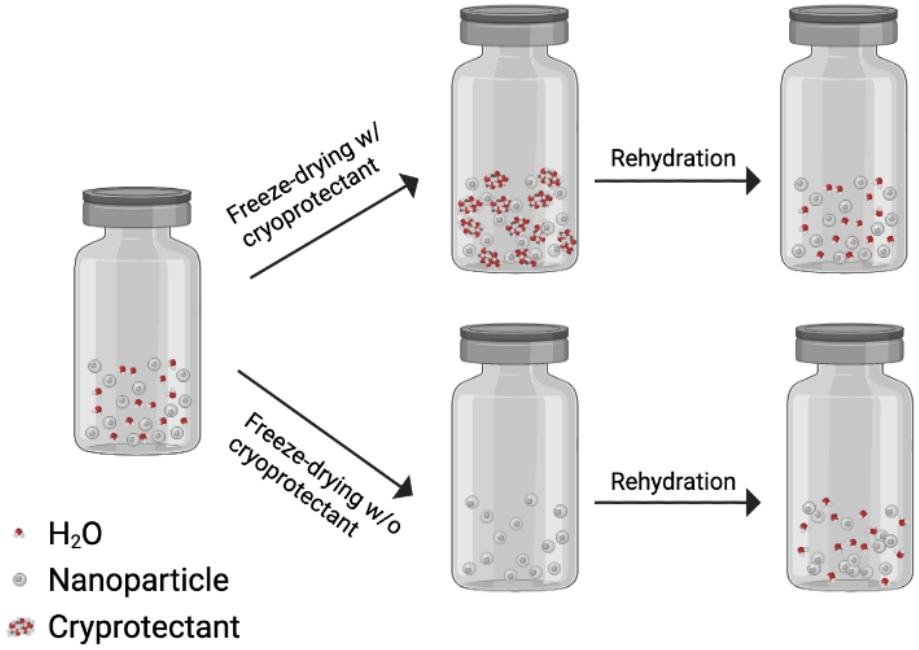

Figure 1.16: *Cryoprotectant's role in prevention of nanoparticle aggregation after reconstitution of lyophilized product. Created with BioRender.com with inspiration from [53].*

Cryoprotectants commonly used for freeze-drying of nanoparticles are sugars such as trehalose, sucrose, and mannitol, and the level of stabilization they can provide depends on their concentrations [64]. Mannitol mainly serves as a bulking agent to obtain an elegant non-collapsed cake, whereas sucrose and trehalose serves as stabilizers in e.g. freeze-dried protein formulations [51].

Anhorn et al. [51] evaluated excipients for freeze-drying and stability of albumin-based nanoparticles. HSA nanoparticles were freeze-dried in the presence of different cryoprotectants (sucrose, trehalose, and mannitol) in different concentrations (1, 2, and 3% (w/v)). Their samples were evaluated with regard to their physiochemical characteristics such as lyophilizate (cake) appearance, particle size, and polydispersity (PDI). These cryoprotective agents showed prevention of aggregation of HSA nanoparticles during freeze-drying and identified as suitable stabilizers, however sucrose and trehalose demonstrated superiority to mannitol. Additionally, the best results from their study were obtained in the presence of 3% trehalose or sucrose, respectively.

In this project, sucrose was selected as the cryoprotectant to be used for lyophilization of nab-mitotane.

Lyophilized drug product – cake appearance

Cake appearance of a freeze-dried product is an important feature which can be critical regarding the product quality (e.g., safety and efficacy). A goal during the design and development of a lyophilized drug product is to achieve a uniform and elegant cake without significant inter- and intra- batch variation. However, sometimes a non-ideal cake appearance (such as shrinkage, cracking, partial collapse) might not impact the product quality. Therefore, the acceptance of a non-ideal cake appearance can be considered. Example of different cake appearances can be viewed in **Figure 1.14**.

Variation in cake appearance is generally classified as either critical, major, or minor, which is based on the impacts the appearance has on patient safety and product efficacy [65].

Particle size is a crucial parameter for the in vivo behavior of the nanoparticles following an intravenous injection [66]. Thus, lyophilization was carried out to get an idea or a first knowledge of how the particle size of nab-mitotane would be influenced by the exposure to stresses associated with freezing, dehydration and rehydration [53] in the presence of a cryoprotectant. Additionally, the intention of the short-term stability study was to gain a first knowledge of the extension in which the particle size of this formulation could be affected over time.

2 Aim of the study

A nanoparticle albumin-stabilized drug formulation has been proposed as a potential formulation for mitotane and is currently being developed. The aim of this project was to optimize the formulation of the albumin-stabilized mitotane (nab-mitotane) as well as evaluating the stability of lyophilized nab-mitotane in a short-term stability study.

In this study, DC were utilized as a method to produce nab-mitotane. Prior to this project, the achieved size with this method resulted in particle size of approx. 350 nm. A way to optimize the nab-mitotane formulation is by reducing the particle size to produce smaller nanoparticles. Therefore, optimizing the method was attempted by experimenting with different parameters that potentially could result in more efficient homogenization and thus producing smaller nanoparticles. For this part of the project, to investigate the influence they have on the particle size, parameters of interest were

- Homogenization aid – the size of the beads, and the amount of beads
- DC processing temperature and time
- pH

The experiments were set up to investigate how a variation of these parameters could affect the degree of homogenization, thus affect the size of the nanoparticles.

Furthermore, the produced nanoparticles will be lyophilized to get a first insight on how the particle size of nab-mitotane could be influenced by the exposure to stresses associated with freezing, dehydration, and rehydration in the presence of a suitable cryoprotectant. Additionally, a short-term stability study will be carried out to get an idea of the stability of freeze-dried nab-mitotane under storage over time. Lyophilization are usually conducted in order to provide a longer shelf-life for the drug product. Will the freeze-dried nanoparticles be able to resist aggregation during lyophilization and storage over time? How will different storage conditions affect the stability during this short-term study? These questions take part in the evaluation of the short-term stability of freeze-dried nab-mitotane.

3 Materials, equipment, and instruments

3.1 Materials

3.1.1 Chemicals

Table 3.1: *List of chemicals used in this project*

Chemicals	Quality / purity	Mw (g/mol)	Source
Bovine serum albumin (pH 5.2)	≥ 96%	–	Sigma-Aldrich, Steinheim, Germany / St. Louis, USA
D(+)-Saccharose	≥ 99.5%	342.30	Carl Roth, Karlsruhe, Germany
D(+)-Trehalose Dihydrate	≥ 99%	378.24	Carl Roth, Karlsruhe, Germany
Ethanol	–	46.07	Carl Roth, Karlsruhe, Germany
Glutaraldehyde 25%	–	100.12	Carl Roth, Karlsruhe, Germany
Mitotane [1-(2-chlorophenyl)-1-(4-chlorophenyl)-2,2-dichloroethane]	≥ 98%	320.04	Sigma-Aldrich, Steinheim, Germany / St. Louis, USA
Sodium hydroxide (1M)	≥ 98%	40.00	Carl Roth, Karlsruhe, Germany

3.1.2 Equipment

Table 3.2: *List of equipment, containers and other supplies used in this project.*

Other materials and equipment	Specifications	Source
Cannulas	Sterican, Gr. 1, 0.90x40 mm, 20Gx1½	B. Braun, Melsungen, Germany
Cellstar® Falcon tubes	15 mL/50 mL, blue screw cap, PP	Greiner Bio-One, Frickenhausen, Germany
Ceramic beads	Type ZY-P Ø: 0.3-0.4mm / 1.4-1.6 mm	Sigmund Lindner GmbH, Warmensteinach, Germany
Crimp Caps for glass vials	N13 (Ø: 13mm), silver, aluminum, center tear off	Macherey-nagel (MN), Düren, Germany
Crimp-neck glass vials (for lyophilization)	Clear, 2.5 mL, Ø outside: 15 mm, 30.5 mm height	Zitt Thoma, Freiburg, Germany
Decapper	For cap seal size Ø: 13 mm	Kebby industries, Rockford, USA
Disposable cuvette	1.5 mL, PMMA	Brand, Wertheim, Germany
Disposable cuvette-lid	LDPE	Carl Roth, Karlsruhe, Germany
Disposable syringe filter	Chromafil Xtra MV-20/25, 0.2 µm pore size	Macherey-Nagel, Düren, Germany
Disposable syringes	3 mL/5 mL, Luer Lock tip; 20 mL, Luer Lock tip	Becton Drive, Temse, Belgium / Franklin Lakes, USA; Servoprax Mediware, Wesel, Germany
Reaction tubes	Attached cap, 2 mL/1.5 mL/ 0.5 mL, natural (transparent), PP	Greiner Bio-One, Frickenhausen, Germany
Laboratory glass bottles	Duran, 100 mL/200 mL	SCHOTT, Mainz, Germany
Micropipettes	Pipetman, 20 µL/200 µL/1000 µL	Gilson, Middleton, USA
Micro tube	2 mL, PP	Sarstedt, Nümbrecht, Germany
Pipette tips	100-1200 µL, blue, PP; 100-1250 µL, transparent, PP; 10 µL/ 200 µL, natural/yellow	Carl Roth, Karlsruhe, Germany; Nerbe plus, Winsen/Luhe, Germany; Greiner Bio-One, Frickenhausen, Germany

Rubber stopper (for glass vials)	Ø: 13 mm, gray, with two legs, butyl rubber	Zitt Thoma, Freiburg, Germany
Thermometer	Red spirit, total immersion, 305 mm, -20 °C to +110 °C	Fisherbrand, Göteborg, Sweden
Vial crimper	Lab-Crimp for Ø: 13 mm crimp caps	Scherf Präzision, Meiningen, Germany

3.1.3 Protective clothing and equipment

Table 3.3: *List of protective clothing and equipment*

Protection gear	**Specifications**	**Source**
Disposable gloves	Nitrile, powder-free, medical examination gloves, PPE category III	Abena, Åbenrå, Denmark
Protective gloves	Latex, PPE category III, for safe handling of chemicals, cytotoxic and biological substances	Berner International, Elmshorn, Germany
Protective gowns	Z+ PLUS, PPE category III, for safe handling of cytostatic drugs	Berner Internatonal, Elmshorn, Germany
Protective sleeves	Cleo Saphir, elastic cuffs	Berner Internatonal, Elmshorn, Germany

3.2 Instruments

Table 3.4: *List of instruments used in this project*

Instruments	**Models and specifications**	**Source**
Analytical balance	Secura224 – 1S; BP 211D; BP-301S (for weighing mitotane)	Sartorius Lab Instruments, Göttingen, Germany
Centrifuge	Centrifuge 5417 R	Eppendorf, Hamburg, Germany
Compressor	Fiac DE 100 F114 oilless	Fiac Air Compressors, Bologna, Italy
Desiccator; porcelain plate; silica gel	–; 188a/140; Silica gel Orange, 2-5 mm	Glaswerk, Wertheim, Germany; Rosenthal Technik, Germany; Carl Roth, Karlsruhe, Germany

Digital thermometer probe	LR44/A76 battery operated	–
Drying oven	Binder ED 23	Hettich, Tuttlingen, Germany
Dual centrifuge	ZentriMix 380 R	Hettich, Tuttlingen, Germany
Freeze-dryer	Alpha 2-4, Christ LOC-1M	Martin Christ, Osterode, Germany
PCS and software	ZetaPals analyzer Zetapals Particle Sizing Software	Brookhaven Instruments Corporation, Holtsville, USA
pH-meter	CG 843 P	SCHOTT, Mainz, Germany
Thermomixer	Thermomixer Comfort	Eppendorf, Hamburg, Germany
Ultrapure water system	Arium pro	Sartorius Lab Instruments, Göttingen, Germany
Ultrasonic bath	Sonorex RK 100	Bandelin, Berlin, Germany
Vacuum pump	Rotary vane pump RZ 6	Vacuubrand, Wertheim, Germany
Vortex Mixer	VM-300	NeoLab Migge, Heidelberg, Germany

4 Methods

The method for the preparation of nab-mitotane was based on a method that is currently not publicly available, as the first paper describing this process has not yet been published. For this reason, in order to refer to this unpublished paper, the parts of the method that were based on that paper will be referenced as [X]. For the lyophilization of nab-mitotane, the parameters set for the freezing and drying steps were based on the freeze-drying of HSA nanoparticles conducted by Anhorn et al. [51].

4.1 Process optimization of nab-mitotane preparation by dual centrifugation

DC performed by the dual centrifuge, Zentrimix 380 R (Hettich, Tuttlingen, Germany), was utilized for the preparation of nab-mitotane, as seen in **Figure 4.2**. This part of the project focused on optimization of the DC method in order to produce nab-mitotane of reduced size, preferably below 200 nm. To do this, some factors that could possibly influence the outcome of the nanoparticle size were experimented with. First, different sizes and amounts of ceramic beads were used as homogenization aid to investigate their influence on the resulting particle sizes. Thereafter, this study explored the influence of the DC parameters such as the temperature and processing time. Finally, the effect of different pH of BSA used to produce nab-mitotane were investigated.

In order to obtain nab-mitotane, the samples containing mitotane, BSA and ceramic beads were homogenized by the dual centrifuge. This was followed by a cross-linking step and a purification step before particle size analysis were conducted. Further details are provided in the coming sections.

4.1.1 Preparing stock solutions

This section describes the preparation of different stock solutions.

To prepare a mitotane stock solution, solid mitotane was weighed and thereafter dissolved in ethanol to a concentration of 20 mg/mL. This stock solution was stored in reaction tubes in the freezer (-30 °C) until use. When mitotane was needed, the stock solution was put in the desiccator for at least 5 min before use [X].

To prepare a BSA stock solution, solid BSA was weighed and thereafter dissolved in purified water obtained by Arium pro ultrapure water system (Sartorius Lab Instruments, Göttingen, Germany). A concentration of 50 mg/mL for stock solution was prepared, and pH was adjusted by the addition of 1 M sodium hydroxide. The solution was filtered through a disposable syringe filter of 0.2 µm pore size and finally stored in falcon tubes in the refrigerator (2-8 °C) until use [X]. Two BSA stock solutions of different pH (one with pH 8.154-8.178 and one with pH 8.998-9.003) were prepared for the purpose of comparison; this will be further described in a later section.

Finally, a stock solution of 8% glutaraldehyde was prepared by diluting 25% glutaraldehyde with purified water [X]. This was stored in reaction tubes in the refrigerator (2-8 °C) until use.

4.1.2 Step 1: Dual centrifugation

Step 1 of the nab-mitotane preparation is the DC. Every sample for a run in the dual centrifuge consisted of 0.25 mL of 20 mg/mL mitotane solution and 1 mL of 50 mg/mL BSA solution (pH 8.154-8.178) until specified otherwise [X]. Mitotane and BSA were pipetted into micro tubes (**Figure 4.2**). Ceramic beads were added as homogenization aid in various amount which will be later specified. Lastly, the samples were placed in a horizontal vial orientation in the dual centrifuge.

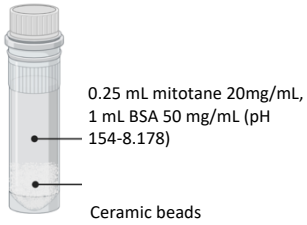

Figure 4.1: *Sample content to produce nab-mitotane by DC.*

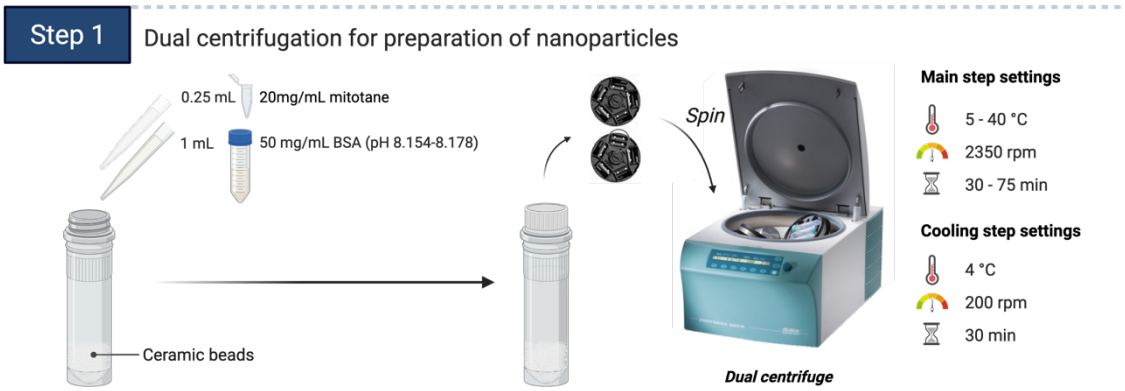

Figure 4.2: *The DC-step to produce nab-mitotane. Created with BioRender.com.*

The DC consisted of a main step followed by a cooling step. The DC parameters set for the cooling step remained constant at 4 °C and 200 rpm for 30 min as a standard [X]. The DC parameters for the main step, however, were varied throughout the project.

In the first set of experiments, different sizes (Ø: 0.3-0.4 mm / 1.4-1.6 mm) and amounts of ceramic beads (300, 750, and 1200 mg) were tested to determine which ones resulted in the smallest particles, an overview given in **Table 4.1**. For the main step, the dual centrifuge was set at 15 °C and 2350 rpm for 30 min, followed by the cooling step.

Table 4.1: *Comparison between different sizes of ceramic beads in addition to different amounts of ceramic beads.*

	Comparison					
Ceramic bead size (Ø)	0.3-0.4 mm			1.4-1.6 mm		
Amounts of ceramic beads (weight)	300 mg	750 mg	1200 mg	300 mg	750 mg	1200 mg
DC settings	Main step: 15 °C, 2350 rpm, 30 min Cooling step: 4 °C, 200 rpm, 30 min					

Moreover, in the second set of experiments, DC parameters such as temperature and process time were varied in the main step. However, the speed was held at 2350 rpm for every experiments. Ceramic beads (1200 mg of Ø: 0.3-0.4 mm) were used as homogenization aid. To investigate the influence of temperature on the particle size, different temperatures (5, 15, 20, 25, and 40 °C) for the main step were tested and maintained for 30 min (**Table 4.2**A). To investigate the influence of processing time, different lengths of time (30, 45, 60, and 75 min) for the main step were set for the DC when the temperature was set at 20 °C (**Table 4.2**B). After every performed main step the cooling step followed.

Table 4.2: *A) Comparison of different temperatures. B) Comparison of different processing time.*

A	**Comparison**				
Temperature	5 °C	15 °C	20 °C	25 °C	40 °C
DC settings	Main step: 2350 rpm, 30 min Cooling step: 4 °C, 200 rpm, 30 min				
Homogenization aid	0.3-0.4 mm (Ø), 1200 mg of ceramic beads				

B	**Comparison**			
Processing time	30 min	45 min	60 min	75 min
DC settings	Main step: 20 °C, 2350 rpm Cooling step: 4°C, 200 rpm, 30 min			
Homogenization aid	0.3-0.4 mm (Ø), 1200 mg of ceramic beads			

Finally, BSA solutions of different pH were used for comparison in the preparation of nab-mitotane, an overview given in **Table 4.3**. BSA solution of pH 8.998-9.003 were run at different processing time (30, 45, 60, and 75 min), and compared with the particle sizes of nab-mitotane obtained when BSA of pH 8.154-8.178 were used in previous experiments.

***Table 4.3**: Comparison between BSA solutions of different pH.*

	Comparison							
BSA (pH)	8.154-8.178 (standard)				8.998-9.003			
Processing time	30 min	45 min	60 min	75 min	30 min	45 min	60 min	75 min
DC settings	Main step: 15 °C, 2350 rpm, 30 min Cooling step: 4°C, 200 rpm, 30 min							
Homogenization aid	0.3-0.4 mm (Ø), 1200 mg of ceramic beads							

4.1.3 Step 2: the cross-linking step

After DC, the samples were incubated to induce the cross-linking of the nanoparticles formed. 11.376 µL of 8% glutaraldehyde (cross-linking agent) was added per sample. The samples were placed into a thermomixer, utilizing Thermomixer Comfort (Eppendorf, Hamburg, Germany) for incubation. The cross-linking process was performed under mixing (500 rpm) at 22 °C for 24h [X], as illustrated in **Figure 4.3** (step 2).

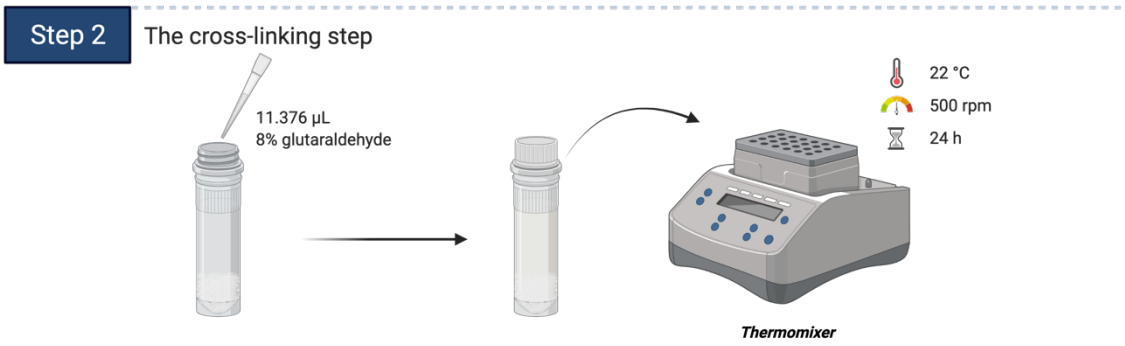

***Figure 4.3:** Incubation to induce the cross-linking process of the nanoparticles. Created with BioRender.com.*

4.1.4 Step 3: Purification of the nanoparticles

After incubation, before the particle size analysis, the resulting nab-mitotane were purified by three cycles of differential centrifugation, as shown in **Figure 4.4**. The centrifugation was operated on the Centrifuge 5417 R (Eppendorf, Hamburg, Germany). One cycle in the purification process consisted of centrifugation, removal of supernatant, addition of purified water, and redispersion of the pellet. These steps were repeated two more times. The parameters for centrifugation were set at a speed of 12 000 x *g* and temperature of 22 °C for 8 min. Afterwards, supernatant was removed by careful pipetting, followed by addition of purified water and redispersion of the pellet. Redispersion was performed through an ultrasonication bath in Sonorex RK 100 (Bandelin, Berlin, Germany) for 5 min (1 min + 3 min + 1 min). During the sonication, after 1 and 3 min, the samples were taken out of the ultrasonication bath and gently shaken by hand before returning for further sonication [X].

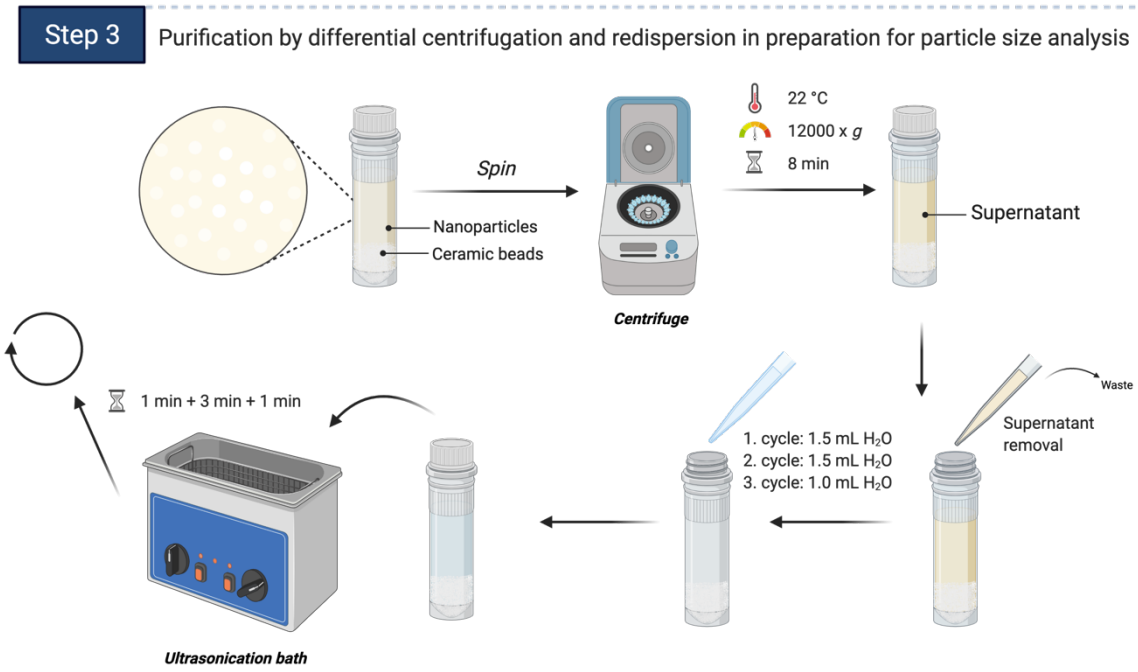

Figure 4.4: *The purification step by three cycles of differential centrifugation and redispersion. Created with BioRender.com.*

4.1.5 Step 4: Determination of particle size and size distribution

After the final redispersion in the purification process, the nab-mitotane were separated from the ceramic beads by pipetting the nanoparticles into a reaction tube (**Figure 4.5**).

The average particle size and PDI of the nab-mitotane were measured by photon correlation spectroscopy (PCS) using ZetaPals Analyzer (Brookhaven instruments corporation, Holtsville, USA). The samples (5 µL) were diluted with 2 mL of filtrated (0.2 µm pore size) purified water in a PMMA cuvette. The parameters set for the analysis were a refractive index at 1.333 and viscosity at 0.933, measured at a fixed temperature of 25 °C and a scattering angle of 90°. Ten measurements were conducted to give an average particle size and PDI [X].

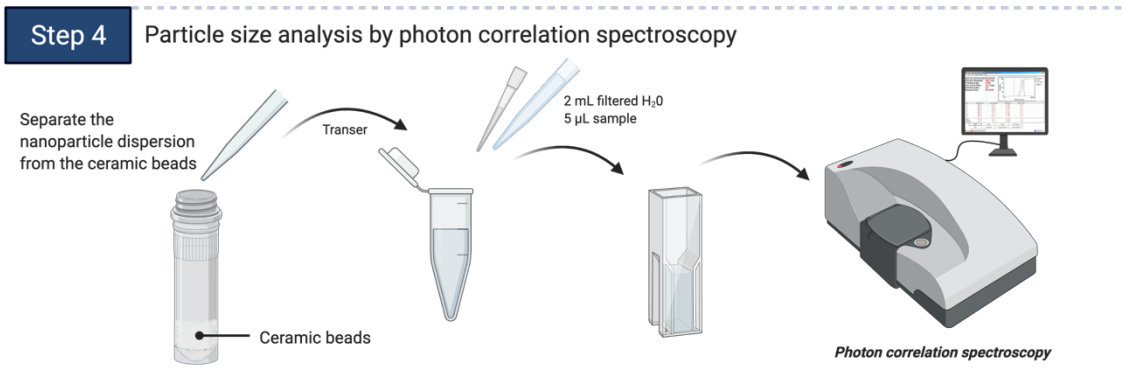

Figure 4.5: *The particle size analysis step, performed by PCS. Created with BioRender.com.*

4.2 Lyophilization for stability improvement of nab-mitotane

For the second part of the project, the nab-mitotane was lyophilized and an evaluation of the stability of freeze-dried nab-mitotane was carried out over a time period of 3 weeks (21 days) in a short-term study.

4.2.1 Short-term stability study

This short-term stability study was carried out to get an idea of the stability of the formulation under storage over the course of 21 days. The freeze-dried nab-mitotane samples were stored at room temperature (20-24 °C) and in the refrigerator (2-8 °C) until the time for reconstitution. Nine samples were prepared and freeze-dried (per replicate), in which each sample were reconstituted on a given day. One sample was reconstituted directly after lyophilization (day 0). Afterwards, two samples (one sample stored at room temperature, and one sample stored at refrigerated temperature) were reconstituted after time periods of 1 day, 7 days, 14 days, and 21 days of storage since lyophilization. Directly after lyophilization and on the different predetermined timepoints, the physicochemical

characteristics such as cake appearance, particle size and size distribution were analyzed, evaluated, and compared in case of any changes over time.

4.2.2 Step 1: Preparing sucrose stock solution and samples for lyophilization

The total volume of one sample to be lyophilized was 350 µL. The nab-mitotane to cryoprotectant volume ratio was 6:1. In this case, sucrose was used as cryoprotectant in a concentration of 6% (w/v). The selection of cryoprotectant and concentration is described in Appendix III. To make a 42% sucrose stock solution, solid sucrose (D(+)-Saccharose) was weighed and thereafter dissolved in purified water. The solution was filtered through a disposable syringe filter of 0.2 µm pore size and finally stored in a reaction tube in the refrigerator (2-8 °C) until use.

Nab-mitotane was prepared by DC as described in **Figure 4.2**, however using BSA with pH 8.998-9.003. For the main step of the DC, the parameters were set at 20 °C and 2350 rpm for 60 min. This was followed by the cross-linking step (**Figure 4.3**), purification (**Figure 4.4**) and particle size analysis (**Figure 4.5**).

A schematic illustration of the sample preparation for lyophilization is shown in **Figure 4.6**. The crimp neck glass vials and rubber stoppers were air blown to remove traces of unwanted particles, and thereafter weighed. A sample was prepared by adding 50 µL of 42% sucrose stock solution (w/v) and 300 µL nab-mitotane into the vial. Lastly, before initiating the lyophilization process, the vial containing sample (sealed with a rubber stopper) was weighed. The sample was briefly vortexed at full speed to mix the content before being loaded into the freeze-dryer. In this project, nine samples were prepared to be lyophilized (per replicate). The sample to be reconstituted directly after lyophilization (day 0) had its rubber stopper replaced by another rubber stopper containing a thermometer probe (vial as depicted in **Figure 1.15**) to monitor the T_p.

The average particle size and PDI of the nab-mitotane samples were measured the same day the lyophilization was initiated, to compare the results before lyophilization with results after lyophilization and reconstitution.

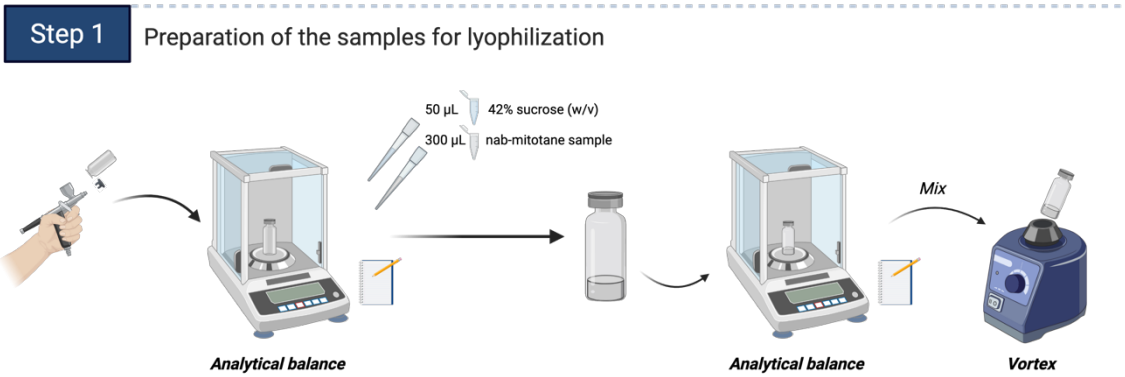

Figure 4.6: *The sample preparation step. The weight of the vial and rubber stopper before and after adding the sample content were noted down. Created with BioRender.com.*

4.2.3 Step 2: The lyophilization process of nab-mitotane

The lyophilization experiments were performed by Alpha 2-4 freeze-dryer (Martin Christ, Osterode, Germany). **Figure 4.7** shows the procedure of the lyophilization process. The samples were loaded into the freeze-dryer, the vials partially unsealed to ensure vaporization and removal of water. With the lid of the freeze-dryer secured shut, the freezing process was initiated. At atmospheric pressure, the shelf temperature was set at -40 °C. These parameters were maintained for 6h [51]. Afterwards, the primary drying step was initiated. The ventilation valve was closed, and the vacuum pump was turned on, reducing the pressure to 0.07 mbar with the safety pressure set at 0.12 mbar. The temperature was increased from -40 to -25 °C. The primary drying went on overnight and lasted for 14.5h, in which the endpoint of primary drying was reached. The shelf temperature was then raised to 25 °C for the secondary drying step. The pressure remained unchanged. These parameters were maintained for 6h [51]. The vials were thereafter sealed completely with the rubber stoppers, ending the lyophilization. The vials were cleaned with ethanol before being placed into the desiccator for 30 min.

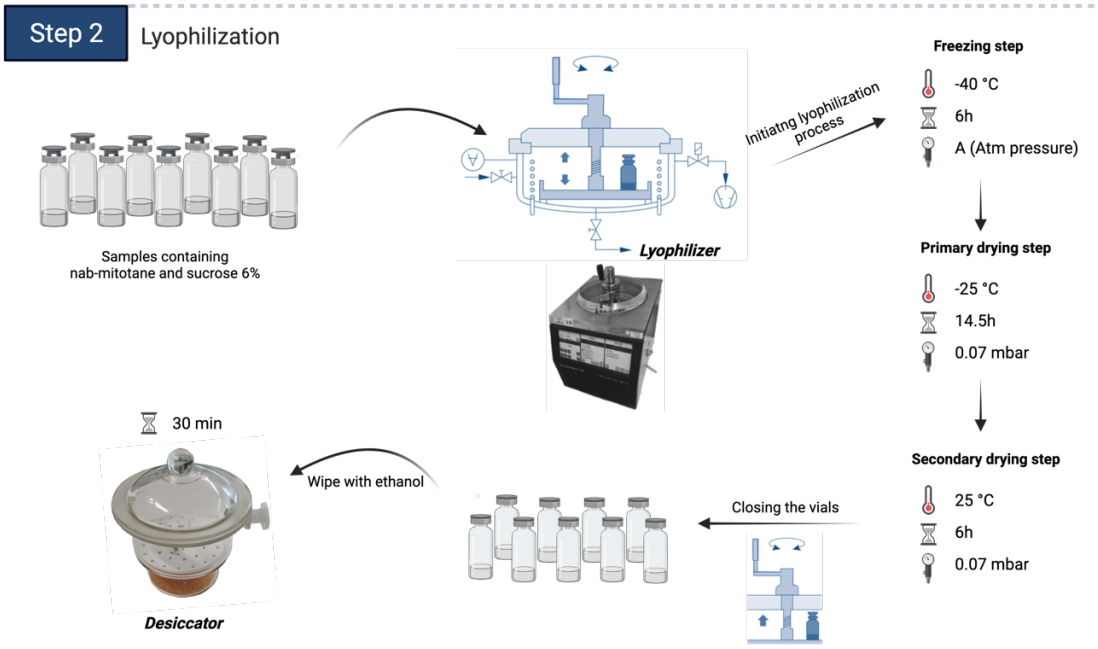

Figure 4.7: *The lyophilization-step starting with a freezing process before going over to the process of drying. After lyophilization, the samples are placed into the desiccator. Created with BioRender.com.*

4.2.4 Step 3: Preparation of the samples for storage

Before storage, the samples were individually weighed. Photos of each sample were taken for the purpose of cake appearance evaluation. Thereafter, the vials (except for the sample to be reconstituted on day 0) were sealed with silver metal caps. Half the number of samples were stored in a drawer at room temperature (20-24 °C), while the remaining half were stored in the refrigerator (2-8 °C) until the day of reconstitution (**Figure 4.8**). The temperature was regularly monitored with a thermometer.

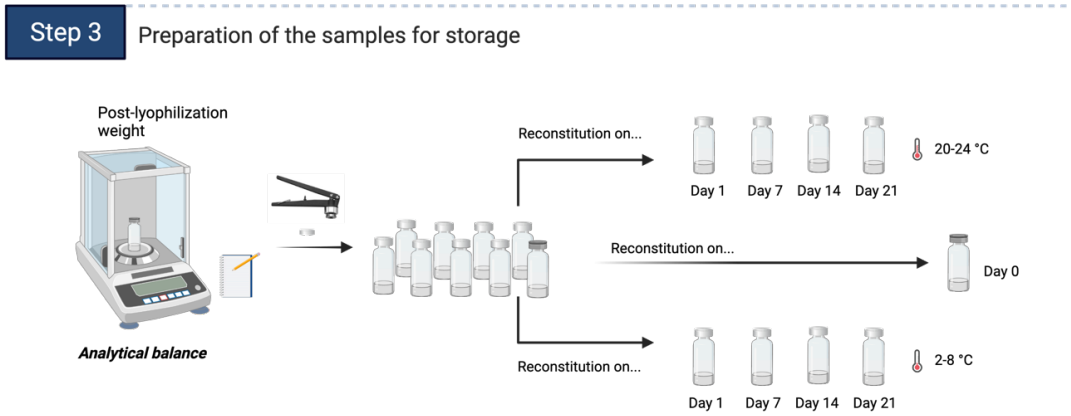

Figure 4.8: *Preparing the samples for storage. The samples are either stored at room temperature or at refrigerated temperature. Created with BioRender.com.*

4.2.5 Step 4A: Reconstitution of the freeze-dried nab-mitotane

The freeze-dried nab-mitotane samples were reconstituted on their predetermined timepoints, as listed in **Figure 4.8**. Before reconstitution, photos of the cakes were taken to be compared to the photos taken on day 0. Then the metal caps were removed using a decapper. Purified water was added to the samples to compensate for the water loss during the drying process. The loss of water was determined by measuring the change in mass of each sample. The sample's initial moisture content was calculated based on **Equation 4.1**.

***Equation 4.1**:*

$$\text{Mass of } H_2O = \text{Initial sample mass} - \text{Final sample mass} =$$

$$\text{Mass}_{\text{(vial + rubber stopper+pre-lyophilization sample)}}\ (g) - \text{Mass}_{\text{(vial + rubber stopper + post-lyophilization sample)}}\ (g)$$

In preparation for particle size analysis, and to ensure proper wetting of the lyophilized cake, the samples were redispersed in the ultrasonication bath for 5 min (1 min + 3 min + 1 min) in the same manner as mentioned in section **4.1.4**. This step is illustrated in
Figure 4.9.

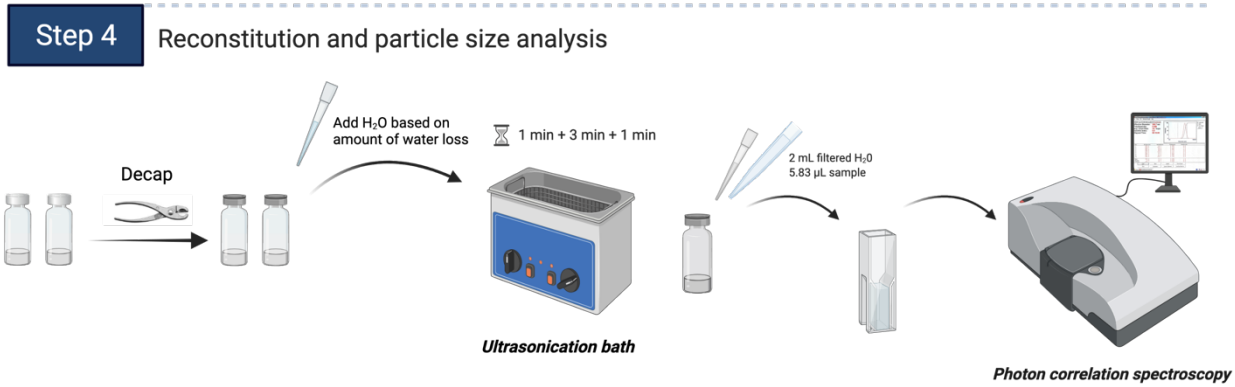

***Figure 4.9:** The reconstitution and particle size analysis step. Created with BioRender.com.*

4.2.6 Step 4B: Determination of particle size and size distribution

Determination of particle size and size distribution of the freeze-dried samples took place after reconstitution (
Figure 4.9) in the same manner as mentioned in section **4.1.5**. However, 5.83 µL of the reconstituted sample were diluted with 2 mL of filtrated (0.2 µm pore size) purified water in a PMMA cuvette.

4.2.7 Evaluation of lyophilized cake appearance

The cake appearance of a sample on the day of reconstitution were compared to the cake appearance directly after lyophilization. The evaluation of the cake appearance was based on the presence of any visible defects such as collapse, cracks, and signs of melting, if any changes in the appearance had occurred during storage. Photos were taken and are provided in the Discussion section.

4.2.8 Evaluation of particle size and polydispersity

Changes in nanoparticle size and size distribution can be an indicator for occurrence of events such as drug leakage, fusion of nanoparticles and aggregation during lyophilization and/or storage [67, 68]. To investigate occurrence of size changes related to the lyophilization process, the particle size and PDI of the samples was measured before- and after lyophilization for comparison. Further on, to investigate occurrence of size changes related to storage over time, the samples were reconstituted on their predetermined timepoints (**Figure 4.8**). The particle size and PDI of these samples were measured and compared with the particle size and PDI obtained from the samples that were reconstituted directly after lyophilization (day 0). Lastly, size changes related to the storage temperature were investigated. The results obtained when samples were stored over time at room temperature were compared to the results obtained when samples were stored over time at refrigerated temperature.

4.3 Statistical analysis

GraphPad Prism was the software utilized to perform statistical tests and to create graphs for comparisons. The values are expressed as mean ± standard deviation (SD), and p-value ≤ 0.05 are considered statistically significant. All graphs also include asterisks representing the p-value classification (**** $p \leq 0.0001$; *** $p \leq 0.001$; ** $p \leq 0.01$; * $p \leq 0.05$; ns $p > 0.05$), based on the significance level (a) at 0.05. The sample size of each experiment was $n \geq 2$.

Examples of statistical tests that were carried out were paired and un-paired t-tests as well as one-way ANOVA tests followed by Dunnett's or Tukey's post hoc test. Two-way ANOVA test followed by Bonferroni's multicomparisons test was also performed. **Table 4.4** lists the different occasions these statistical tests were used.

Table 4.4: *The statistical tests that were used on the different experiments for comparison.*

Process optimization of nab-mitotane preparation by dual centrifugation	
Comparison experiments	**Statistical test utilized**
Different amounts of ceramic beads (three groups)	One-way ANOVA followed by Tukey's post hoc
Different sizes of ceramic bead at different amounts of beads (two factors, two groups)	Two-way ANOVA followed by Bonferroni's multicomparisons test
Different sizes of ceramic beads (two groups)	Paired t-test
Different temperatures (five groups)	One-way ANOVA followed by Tukey's post hoc
Different lengths of processing time (two-three groups)	Two groups: Unpaired t-test Three groups: One-way ANOVA followed by Tukey's post hoc
BSA solutions of different pH (two groups)	Paired t-test
Lyophilization study and short-term stability	
Comparison experiments	**Statistical test utilized**
Before and after lyophilization (two groups)	Paired t-test
Comparing day 0 with day 1, 7, 14, and 21 (five groups)	One-way ANOVA followed by Dunnett's test
Comparing samples stored at room temperature with samples stored at refrigerated temperature over time (two factors, two groups)	Two-way ANOVA followed by Bonferroni's multicomparisons test

5 Results and discussion

The binding of mitotane to albumin nanoparticles for an intravenous application could be a promising formulation strategy to circumvent the therapy-limiting effect associated with the current available formulation (tablet). The method developed for the preparation of nab-mitotane utilizes the DC-technique. However, this method led to nanoparticles with a mean diameter of approx. 350 nm [X]. As an exogenous substance, these nanoparticles are therefore considered as foreign and are susceptible for opsonization and elimination by the activation of the lymphatic system [28]. Thus, this project focused on formulation optimization through the optimization of the DC method to reduce the particle sizes. Additionally, lyophilization of nab-mitotane was carried out for a short-term evaluation of their stability.

5.1 Dual centrifugation – particle size and size distribution

Based on the results that will be presented in this section, the most promising parameters for nanoparticle preparation were selected for further investigations.

5.1.1 The influence of ceramic beads on the particle size

The influence of different amounts of beads

The results in form of particle size and PDI obtained from using different amounts of beads (300 mg, 750 mg, and 1200 mg) are shown in **Figure 5.1**.

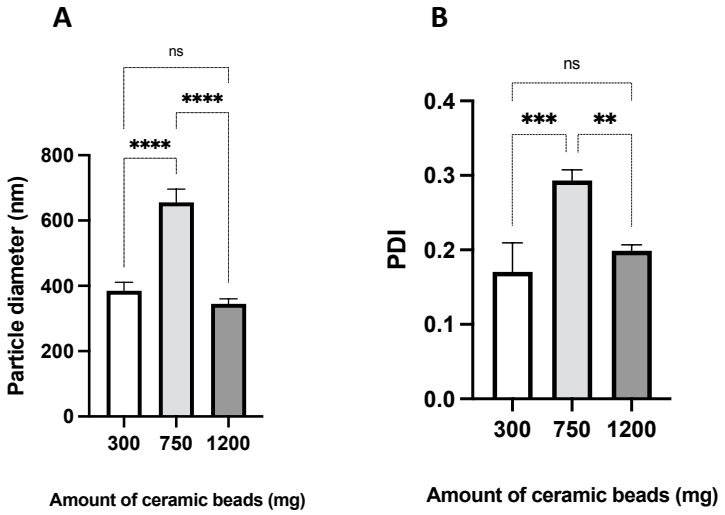

Figure 5.1: A) *Mean particle size and* ***B)*** *mean PDI of nab-mitotane obtained when using different amounts of ceramic beads (Ø: 0.3-0.4 mm) (mean ± SD, n = 4 (300 mg and 1200 mg) and 3 (750 mg)).*

Based on a one-way ANOVA, the overall difference between the use of the different amounts of ceramic beads (Ø: 0.3-0.4 mm) was found to be statistically significant. However, following a Tukey's post hoc test, the differences were only significant when compared with 750 mg beads.

Up to a certain point, regarding the impact on particle size, one can assume to observe a trend of either increasing or decreasing size following an increasing addition of ceramic beads. However, the degree of homogenization depends on other factors as well, such as the type and amount of sample, the type and size of beads, and if there is enough space for the beads to move freely to impact the sample [69]. It has been reported that an increase in number of beads can induce more bead-bead interactions that can efficiently reduce the size of the particles, given that the beads have enough room for thorough homogenization [48]. Hagedorn et al. [49] reported as such; i.e. a higher amount of ceramic beads resulted in a more efficient milling of particles. Thus, it can be expected that the increase in the number of beads can provide efficient homogenization up to the point where the remaining space in the vial limits the movement of the beads and the mixing of sample. From there, it can be thought that a further increase in number of beads could lead to a less efficient homogenization due to overfilling of the vial [69]. In this experiment, the use of 300, 750 and 1200 mg of ceramic beads was investigated to determine which one would result in the most efficient homogenization (smallest particle).

Interestingly, while the comparison between the use of 300 and 1200 mg beads were statistically insignificant, the use of 750 mg beads seem to result in significantly bigger particles with increased polydispersity as shown in **Figure 5.1** (or **Table S 2** for p-values). In all three repetitions that were

conducted with the use of 750 mg beads (n = 3), the particle size analysis led to a mean particle diameter of more than 600 nm in every case. Another interesting observation, based on a currently unpublished work prior to this project [X], is that an amount of 600 mg of ceramic beads usually led to an average particle size of approx. 350 nm. One could assume, if not for the current results provided when using 750 mg beads, that there might be a decreasing trend regarding the particle size when increasing the number of beads from 300-1200 mg. It is difficult to know for certain what might have caused the unexpected significant increase in particle size when using 750 mg of beads as compared to 300 and 1200 mg beads. However, it is recommended to further investigate this by repeating the experiments for clarification as it is not possible to conclude a correlation between amount of beads and particle size.

While the influence on the particle size and PDI is insignificant when using 300 mg beads compared to 1200 mg beads (**Figure 5.1**), 1200 mg beads were selected for the next experiments. The choice was based on earlier findings, in which a higher amount of beads could result in improved homogenization [49] due to more bead-bead interactions [48], provided that there is enough room for the beads to mix the sample material efficiently [69].

The influence of ceramic bead size

The results in form of particle size and PDI obtained from using different bead sizes (diameter of 0.3-0.4 mm and 1.4-1.6 mm) are shown in **Figure 5.2**.

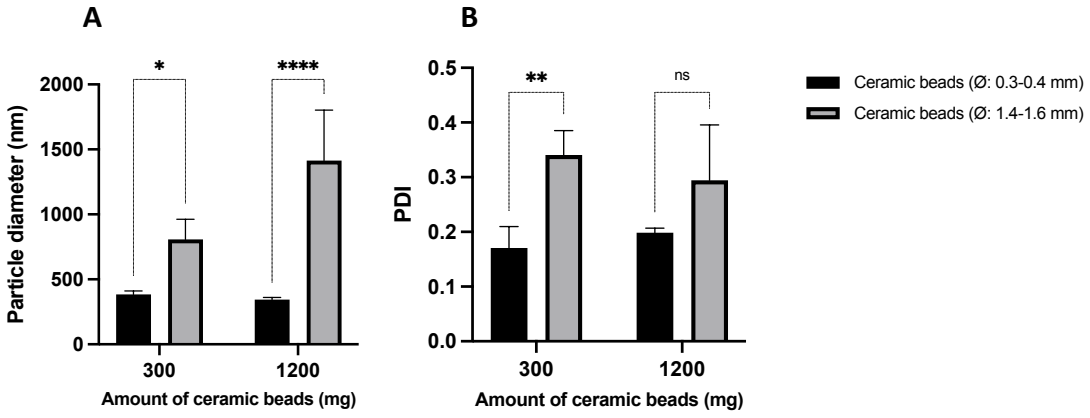

Figure 5.2: A) *Mean particle size and* ***B)*** *PDI of nab-mitotane obtained based on the use of different sizes of ceramic beads and different amounts of ceramic beads (mean ± SD, n = 4 (Ø: 0.3-0.4 mm) and 2 (Ø: 1.4-1.6 mm)).*

A two-way ANOVA followed by a Bonferroni's multicomparisons test was conducted to determine if the outcome of using ceramic beads with a diameter of 1.4-1.6 mm would differ significantly from the outcome of using beads with a diameter of 0.3-0.4 mm. Two independent factors were set up for the comparison, one of which was the bead size, while the other was the amounts of beads (**Figure 5.2**). Thus, the outcome obtained from using 300 and 1200 mg of 1.4-1.6 mm (Ø) beads were compared to the outcome obtained when using the corresponding masses of 0.3-0.4 mm (Ø) beads. The values collected from the previous experiment when testing the influence of different amounts of bead (Ø: 0.3-0.4 mm) on the particle size are also used for this experiment. However, due to the unexpected outcome when 750 mg beads were used in the production of nanoparticles, these results were excluded from further comparisons.

Regarding the influence of bead size on the particle size, due to the presence of an interaction ($p = 0.0021$), the bead sizes have different effects on the particle size depending on the amount of beads. More precisely, any differences between bead sizes has different effects on the particle size depending on the amount of beads [70]. This makes it difficult to interpret the overall effect of bead size on the particle size. Thus, a Bonferroni's multicomparisons test was conducted (**Table S 3** for adjusted p-values). There was found a significant difference in the particle sizes obtained when using 300 mg beads with diameter 0.3-0.4 mm compared to 300 mg beads with diameter 1.4-1.6 mm. Similarly, the use of 1200 mg beads of the two different bead sizes resulted in significantly different particle sizes. This indicates that bead size has the ability to influence the degree of homogenization during the DC. Additionally, based on **Figure 5.2A**, the smaller bead size resulted in the production of significantly smaller particles. These findings agree with existing publications that have similarly reported an improved homogenization associated with smaller beads. According to Massing et al. [48], an increase in number of beads while keeping the bead mass constant can result in more collision between beads as well as amplifying the motion (and thus mixing) of the sample. The more beads that are able to move through the sample material, the more bead-bead interactions can take place and provide optimized homogenization, i.e., if the viscosity of the sample allows the beads to easily move through the sample material. This tendency can be reflected in this experiment. For example, a mass of 300 mg beads leads to a greater number of beads when utilizing smaller beads compared to bigger ones. Furthermore, by increasing the amount of beads to 1200 mg, a far greater number of beads are adding up with the smaller beads than with the bigger beads. The increased number of beads provides many more bead-collisions that can break down particles to smaller sizes.

Regarding the influence of bead size on the PDI, there was found no significant interaction between bead sizes and amounts of beads. More precisely, any differences in PDI when using different bead

sizes are independent on the amount of beads, thus making it possible to interpret the overall influence of different bead sizes on the PDI. In this experiment, the influence of different bead sizes on the PDI was statistically significant. However, Bonferroni's multicomparisons test identified only a significant difference when using 300 mg beads, whereas using 1200 mg beads were insignificant (**Figure 5.2B**).

To summarize, there have been multiple indications in which suggests that smaller beads tend to produce smaller particles. For example, the influence of different bead sizes on the particle size was statistically significant, in which the use of smaller beads (Ø: 0.3-0.4 mm) resulted in smaller particles compared to the use of bigger beads (Ø: 1.4-1.6 mm) (**Figure 5.2A**). Similar observation was seen regarding the influence of 300 mg of different bead sizes on the PDI (**Figure 5.2B**). Additionally, despite the insignificant differences on the PDI when 1200 mg beads were used, it does not indicate that the use of bigger beads could be more beneficial than the use of smaller beads. Furthermore, as mentioned, earlier findings suggest an increase in number of beads while keeping the bead mass constant (by using smaller beads) result in more bead-bead interactions that can contribute to a further reduction of particle diameter [48]. Thus, smaller beads could be more favorable.

5.1.2 The influence of temperature on particle size

The results in form of particle size and PDI obtained from samples operated on different DC processing temperatures (5, 15, 20, 25, and 40 °C) are shown in **Figure 5.3**.

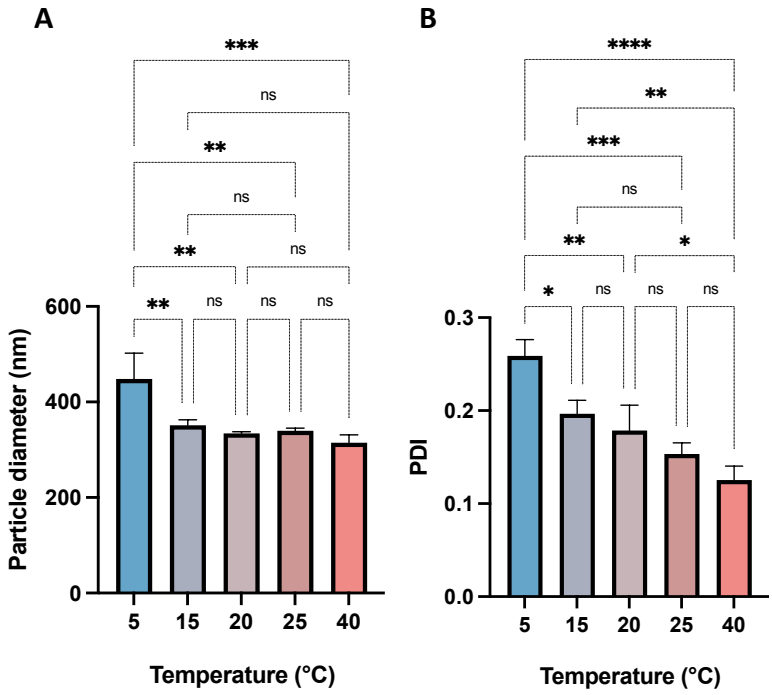

Figure 5.3: A) *Mean particle size and* ***B)*** *mean PDI of nab-mitotane obtained when different processing temperatures were applied during DC (mean ± SD, n = 3).*

A one-way ANOVA followed by Tukey's post hoc test were conducted to determine if a variation in temperature during the preparation of nab-mitotane could affect the particle size and PDI.

Regarding the influence of temperature on the particle size, a significant difference was observed between the different operated temperatures. The outcome following a Tukey's multicomparisons test are shown in **Figure 5.3A** (or **Table S 4**). While there are no significant changes in particle size with temperatures above 15 °C, an increase in particle size seem to occur with temperatures below 15°C. Samples processed at 5 °C seems to differ significantly from all the other temperatures. Although tested at different temperatures, this has a similar trend as reported by Steiner et al. [71], in which positive effects (a decrease in size) can come of higher process temperatures. This might be due to changes in viscosity, for which increased temperature is associated with increased kinetic energy. Increased kinetic energy reduces the intermolecular forces between molecules, and thus can decrease the viscosity [72]. Hence, higher temperatures can make it easier for e.g., homogenization aid to move through the sample material. Furthermore, the increased flowability by the decreased viscosity can have an effect on the movements of the sample material within the vial as well as the impact of the material to the walls of the container.

Regarding the mean PDI, a significant difference was also observed between the different operated temperatures. As shown in **Figure 5.3B**, a decreasing tendency in size distribution can be seen. However, significant differences were mostly associated with processing temperatures when comparing with 5 and 40 °C. Again, this is reflected in the experiments conducted by Steiner et al. [71], in which the lowest PDI are seen at highest operated temperature (40 °C), with a tendency of increasing PDI with decreasing temperature. While there are no significant differences in particle size between processing temperature of 40 °C and the other temperatures (apart from 5 °C), processing the DC at 40 °C resulted in the smallest particles in this experiment, with a mean diameter of 314.8 $\pm$ 16.5 nm. This might explain the lowest PDI value, due to a more homogenous size distribution.

In the end, 20 °C was the selected temperature for further studies. This is due to different reasons. For example, energy is brought into the samples through the application of shear forces during the DC, resulting in powerful sample movements. This contributes to a temperature increase in the sample [48]. To avoid the possibility of a further increase in temperature that might result in destruction of sample, 20 °C were chosen. Additionally, an increase in processing temperature did not seem to lead to a further reduction of the particle size (**Figure 5.3A**). Despite that a processing temperature at 40 °C led to a significant different PDI obtained compared to when 20 °C were operated, 20 °C were selected also based on time efficacy. With 40 °C, the dual centrifuge needed time for pre-heating before initiating the DC of the samples. Still, it would be interesting to further investigate the processing temperature at 40 °C (as the maximum temperature that can be operated on the dual centrifuge) for future studies.

5.1.3 The influence of processing time on particle size

The results in form of particle size and PDI obtained from samples operated on different DC processing times are shown in **Figure 5.4**. **Figure 5.4A** and **C** shows the results obtained when samples contained BSA of pH 8.154-178, and **Figure 5.4B** and **D** shows the results obtained when samples contained BSA of pH 8.998-9.003.

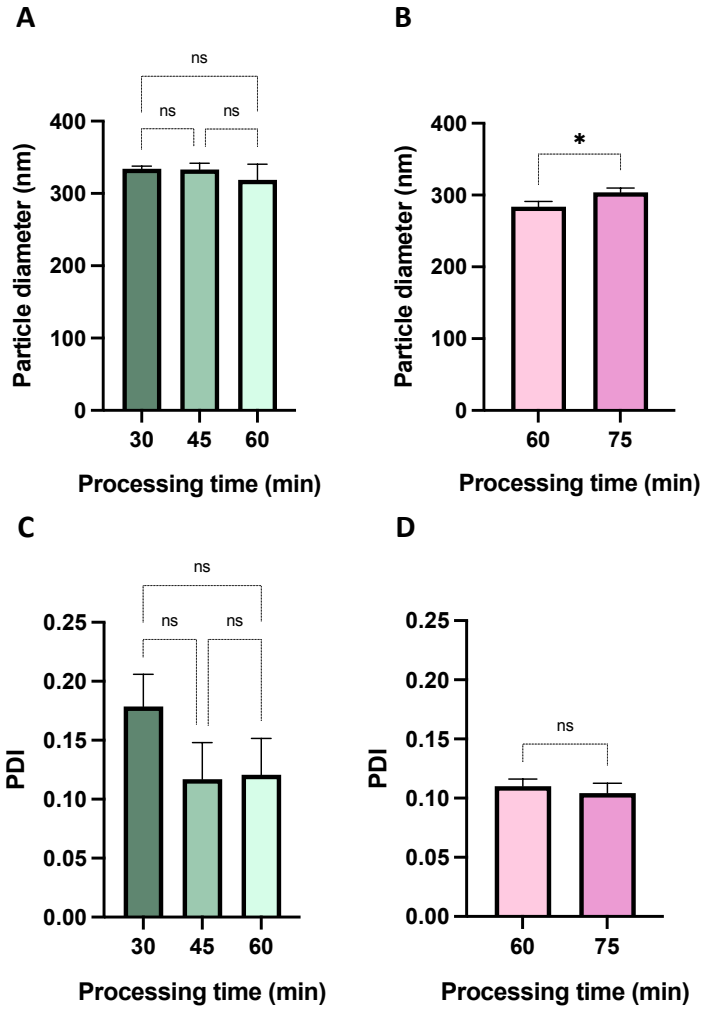

***Figure 5.4**: **A) B)** Mean particle size and **C) D)** mean PDI of nab-mitotane obtained at different processing time during DC. **A)** and **C)** use BSA of pH 8.154-8.178, and **B)** and **D)** use BSA of pH 8.998-9.003 (mean ± SD, n = 3).*

A one-way ANOVA was conducted for the experiment that used BSA of pH 8.154-8.178 due to three comparable groups. An un-paired t-test was utilized for the experiment that used BSA of pH 8.998-9.003 due to only two comparable groups. These statistical tests were conducted to determine whether a variation in processing time could influence the particle size and PDI. Results following the one-way ANOVA showed a nonsignificant difference between the different operated lengths of processing time, for both particle size and PDI. However, following an un-paired t-test to compare 60 with 75 min when BSA of pH 8.998-9.003 was used, a significant difference in particle size was observed between the two groups. In this case, a processing time of 60 min when BSA of pH 8.998-9.003 was used seems to result in smaller particles (**Figure 5.4B**). There was otherwise observed no significant difference regarding the PDI.

It can be expected that increased processing time can affect the particle size and size distribution due to the prolonged mechanical stress induced by the grinding media. Furthermore, due to these

stresses in addition to the input of energy to the sample through the application of shear forces for DC, the temperature will rise within the sample. These factors might contribute to a decrease in particle size. Several papers reported that the influence of process time can occur, but only to a certain extent [48, 49, 71].

Based on the results (**Figure 5.4)**, a processing time of 60 min when BSA of pH 8.998-9.003 was used seems to be favorable. In the next experiment, the difference between the use of BSA solution with pH 8.154-8.178 and pH 8.998-9.003 was investigated, processed for 60 min.

5.1.4 The influence of pH on particle size

The results in form of particle size and PDI obtained from using BSA solutions of different pH (pH of approx. 8 and 9) in the preparation of nab-mitotane are shown in **Figure 5.5**.

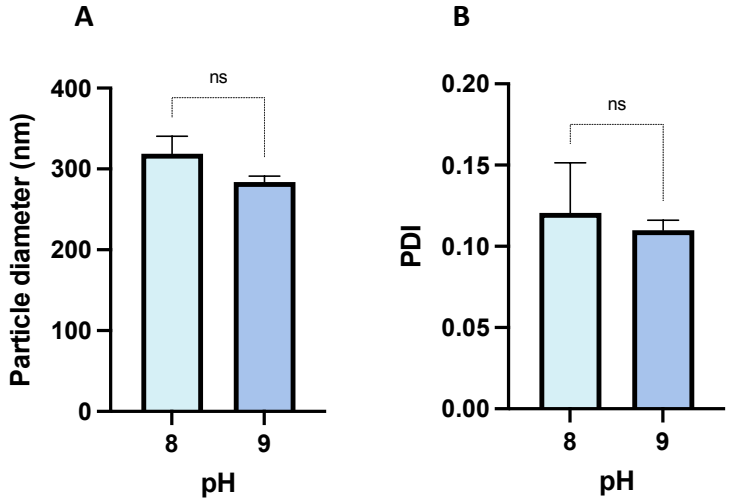

Figure 5.5: ***A)*** *Mean particle size and* ***B)*** *mean PDI of nab-mitotane obtained when BSA solutions of different pH were used (mean ± SD, n = 3). pH 8 = 8.154-8.178; pH 9 = 8.998-9.003.*

For this part of the project, it was assumed that an increase in pH might lead to a decrease in particle size. It has been reported by Langer et al. [66] that higher pH values of HSA solutions could lead to smaller nanoparticles when comparing aqueous HSA solutions at pH values between 7-9. Thus, considering that HSA is stable in the pH range 4-9, the use of BSA of pH 8.154-8.178 were compared with BSA with pH of approx. 9. Conversely, the results following a paired t-test showed no significant differences between the use of BSA solutions with different pH, neither in particle size nor PDI. It might be beneficial to conduct more experiments to clarify the influence of pH on the particle

diameter. Furthermore, additional groups with a greater variation in pH value could be interesting, by for example comparing BSA solutions with different pH in a range between 4 and 9. However, despite the insignificant difference between the particle sizes and PDIs obtained between the BSA solutions of different pH, the BSA solution of higher pH value (8.998-9.003) was selected as a parameter for further experiments. This is due to reported findings that suggested a decrease in particle diameter with increasing pH of HSA solution [66].

5.1.5 Dual centrifugation method optimization – summary

To summarize this part of the project, different experiments were conducted in the attempt to optimize the homogenization of nab-mitotane by the method of DC. Based on the results, the following parameters were selected as the most suitable in obtaining smaller nanoparticles in this project: BSA solution adjusted to a pH of approx. 9 were used in the preparation of nab-mitotane, in which the samples were processed at 20 °C and 2350 rpm for 60 min for the main step of the DC. 1200 mg ceramic beads with a diameter of 0.3-0.4 mm were added as homogenization aid. The selection was based on statistical proof of being significant different from their comparing groups, in which was additionally supported by earlier findings. In cases where differences were statistically insignificant, the selection was based on earlier findings and reported potentials described in publications. With these parameters, a mean particle size and PDI of 282.2 ± 9.2 nm and 0.119 ± 0.021 ($n = 12$) were achieved, respectively. By comparing the mean particle size of 282.2 nm with a theoretical mean of 350 nm in a one-sample t-test, the obtained particle size was considered significantly different from the reference ($p < 0.0001$).

Preparation of nab-mitotane with these parameters were used in further experiments that involved lyophilization of the nanoparticles to conduct a short-term stability study. The result will be presented in the next coming sections.

5.2 Lyophilization – cake appearance, particle size and size distribution

A short-term stability study of freeze-dried nab-mitotane was carried out for 21 days to evaluate the stability upon storage over time.

5.2.1 The cake appearance of lyophilized product over time

Figure 5.6 shows the cake appearance of each sample, showing the appearance directly after lyophilization (day 0) and on the assigned day for reconstitution. Based on the cake appearances obtained directly after lyophilization, there are several differences that can be observed between some of the samples. For example, some samples have formed a partial lyo-ring (such as sample R7, R14 and F14). Furthermore, all samples have some fine powder of product on the inside of the vial wall. Lastly, some of the samples have product between the vial and the rubber stopper (such as sample F1, R14, F14, R21 and F21). However, there are no visible signs of e.g., cracks, collapse or melting.

The evaluation of whether the appearance of the cakes is acceptable or not is based on some general considerations that are summarized in a publication by Patel et al. [65]. The authors give an overview of cake appearances that can be considered acceptable due to no influence on the product quality. They have also listed different cake appearances that should be rejected for various reasons, for which all of them have an impact of the product quality. If the cake appearance indicate that the product quality has been affected, then the cake is consequently rejected due to a possible effect on patient safety and product efficacy.

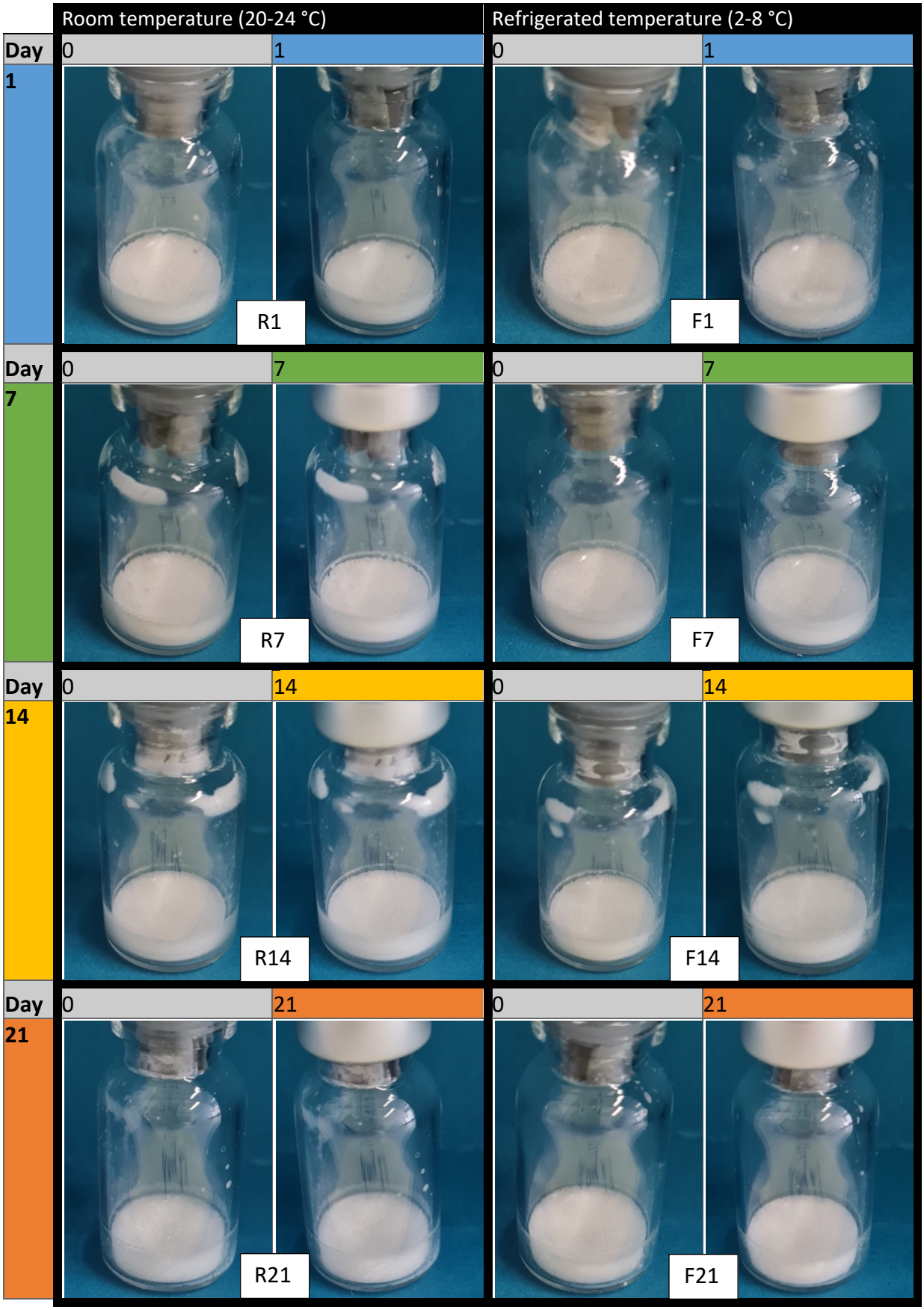

Figure 5.6: *Lyophilized cakes. Photos of the cake appearance of each sample were taken on day 0 and on the assigned day for reconstitution. n = 2. Photo: Cindy Zhang.*

After an evaluation of the cakes seen in **Figure 5.6**, the cause of the appearances in all cases is likely due to the agitation of the vial and sample after the filling process, i.e., the samples were vortexed before loading into the lyophilizer. Consequently, traces of sample material were present around the neck and/or on the inside wall of the vials that did not have time to fall back into the bulk solution at the bottom of the vial. For parenteral application, the samples with product near the opening of the vial are associated with risks concerning sterility and dose accuracy, thus contributing to endangerment of patient, and are therefore not accepted. Other than that, lyo-rings and product on the wall do not compromise the product quality and are thus acceptable.

Further on, there has not been observed any noticeable change in the cake appearance over the time the samples were under storage, neither in the shape, texture nor color.

For this part of the project, there were originally produced three replicas for the stability study. However, one of them was compromised due to technical issues, leading to an interruption of the freezing process. Consequently, cracked cakes were the end outcome (**Figure 5.7**). Due to this deviation from the original plan for the freezing process, these samples were excluded from the replicas. Thus, the overall stability evaluation was based on a sample size of n = 2.

Figure 5.7: *Photos of cracked lyophilized cakes due to issues during the freezing process. Photo: Cindy Zhang.*

5.2.2 Particle size and size distribution

Before the initiation of the short-term stability study, the selection of suitable concentration of the sucrose (cryoprotectant) was investigated. Results from this experiment are presented in Appendix III.

Further on, this section will provide results from experiments that investigated the effect of lyophilization on the particle size of nab mitotane. Additionally, the influence of storing the freeze-dried samples over time in different storage conditions were evaluated.

Before and after lyophilization

This experiment investigated the influence of the lyophilization process on the particle size of nab-mitotane. The results in form of particle size and PDI obtained before and after lyophilization are shown in **Figure 5.8**.

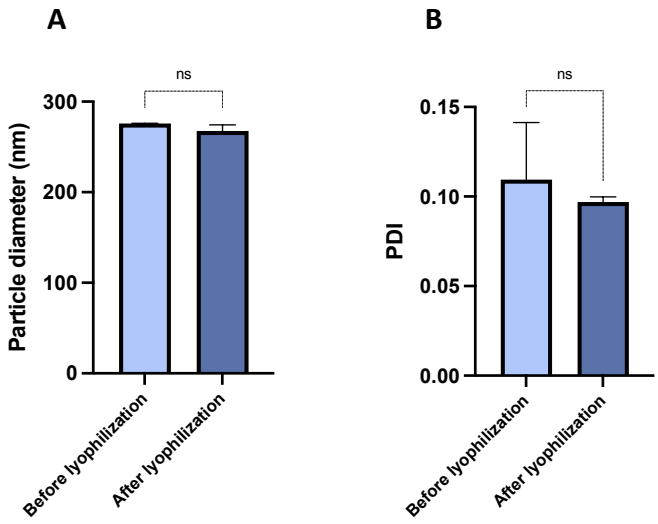

Figure 5.8: A) *Mean particle size and* ***B)*** *mean PDI of nab-mitotane before and directly after lyophilization and reconstitution (mean ± SD, n = 2).*

A paired t-test was performed for comparison between the results obtained before and after the freeze-drying. As demonstrated in **Figure 5.8**, there were no significant changes when nab-mitotane was lyophilized with 6% sucrose (w/v) as cryoprotectant. This observation indicated prevention of particle aggregation that is usually associated with stresses caused by the freezing and drying processes [64]. Thus, the maintenance of both particle diameter and polydispersity indicated stable nanoparticles. Whether this was due to the added cryoprotectant was not demonstrated because of the lack of control (lyophilization of sample without cryoprotectant). However, Anhorn et al. [51] demonstrated that the presence of sucrose at a sufficient concentration (compared to the absence) could preserve the HSA nanoparticles from aggregation during the freeze-drying and subsequent reconstitution. This indicates that the preserved particle size of nab-mitotane was likely due to sucrose.

Stability after storage at room- and refrigerated temperature

The results in form of particle size and PDI obtained after lyophilization and subsequent reconstitution over the course of 21 days are shown in **Figure 5.9** for samples that were stored at room temperature.

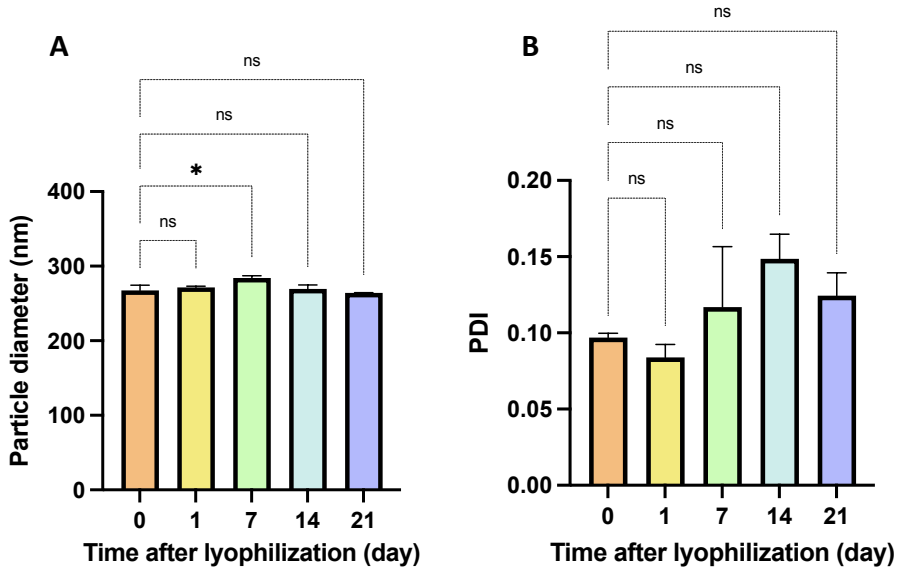

Figure 5.9: A) *Mean particle size and* ***B)*** *mean PDI of nab-mitotane, measured after lyophilization and reconstitution over a time period of 21 days and stored at room temperature (mean ± SD, n = 2).*

To investigate any significant changes regarding the particle size and PDI over the course of 21 days, a one-way ANOVA was carried out. This resulted in an overall p-value that indicated a significant change in particle size had occurred over time. After conducting a Dunnett's post hoc test with day 0 as control, only the comparison between day 0 and day 7 showed to be statistically significant regarding the particle size. One would expect that, should particle aggregation occur, an increase in both particle size and size distribution would be observed over time. **Figure 5.9A** shows a slight increase in size after 7 days of storage at room temperature. Contradictory, the outcome from day 14 and 21 remained statistically nonsignificant when compared to day 0. It is difficult to be certain over the cause of this increase in size only for day 7. However, due to the fact that longer storage time would typically lead to larger and more polydisperse particles [51], this might owe to the fact that this experiment had a small sample size (n = 2). Further investigation is needed for this stability study at room temperature to obtain more conclusive results.

As for samples that were stored in the fridge, the results are shown in **Figure 5.10**.

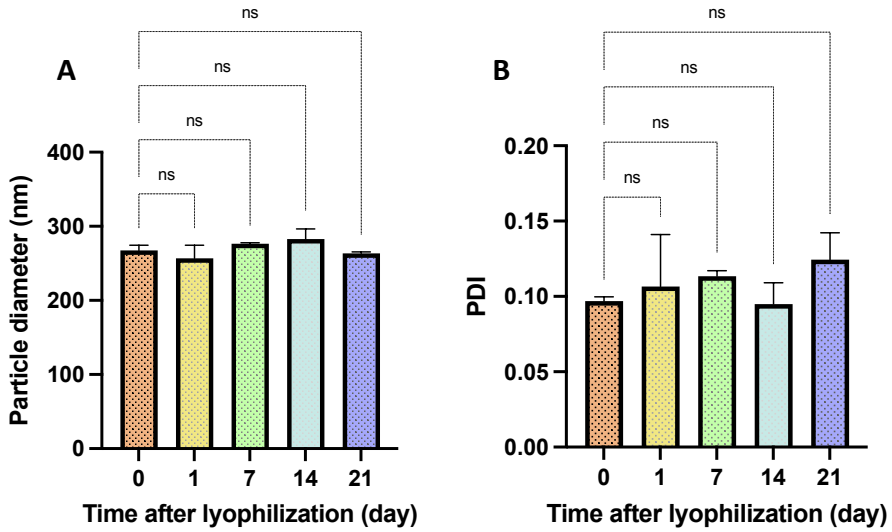

***Figure 5.10**: **A)** Mean particle size and **B)** mean PDI of nab-mitotane, measured after lyophilization and reconstitution over a time period of 21 days and stored at refrigerated temperature (mean ± SD, n = 2).*

Anhorn et al. [51] reported that a concentration of 3% sucrose (or trehalose) (w/v) represents an optimal formulation for long-term storage of freeze-dried HSA nanoparticles (10 mg/mL). They observed no influence on particle size and PDI in the presence of the mentioned cryoprotectants over the 13 weeks the stability study was conducted. They further suggested that these nanoparticles have the potential to be stored at 2-8 °C, and maybe even at 25 °C, for several months. Similar to their work, the experiment conducted here following a one-way ANOVA showed no statistical changes in both particle size and PDI. This is a promising indication that storage at refrigerated temperature has little influence on the particle size and PDI (at least short-term) in the presence of a sufficient concentration of sucrose. Contrast to their findings, there was a significant difference in particle size between day 0 and 7 when the samples were stored at room temperature (20-24 °C) (**Figure 5.9A**).

The effect of different storage temperature on the stability

Samples that were stored at room temperature was compared with samples that were stored at refrigerated temperature. Each set of results in form of particle size and PDI obtained after lyophilization and subsequent reconstitution over the course of 21 days are shown in **Figure 5.11.**

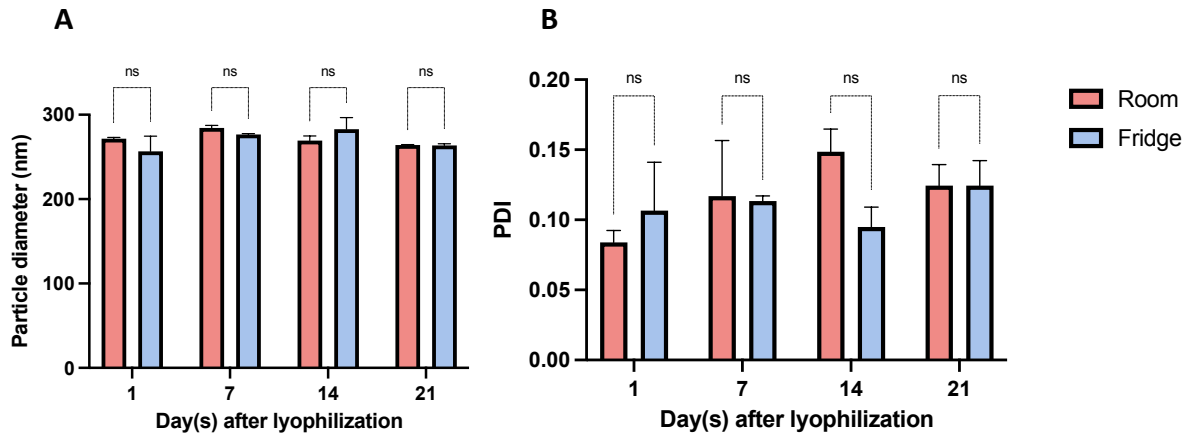

Figure 5.11: A) *Mean particle size and* ***B)*** *mean PDI of nab-mitotane, measured after lyophilization and reconstitution over a time period of 21 days and stored at room temperature (red bars) and refrigerated temperature (blue bars) (mean ± SD, n = 2). Results from storage at room temperature were individually compared to results from storage at refrigerated temperature at corresponding days.*

To be able to compare the particle size and PDI between the storage conditions over time, a two-way ANOVA followed by Bonferroni's multicomparisons test was carried out. Results are presented in **Figure 5.11**. No significant differences were observed when freeze-dried nab-mitotane was stored at room temperature compared to in the refrigerator.

Prior to this experiment, it was expected that storage at lower temperatures would be better at preserving the stability due to the nature of albumin as a protein. There have been suggestions of the possibility of storing lyophilized BSA at room temperature for up to 3 weeks [73]. However, storage at room temperature often leads to increased levels of protein degradation/inactivation and microbial growth that could compromise the stability. Therefore, it is commonly recommended for proteins to be stored at refrigerated temperatures, alternatively in a frozen state for long-term storage [74]. Unlike expected, this experiment showed no significant differences when freeze-dried nab-mitotane was stored at room temperature compared to refrigerated samples. Additionally, as mentioned in the previous section, Anhorn et al. [51] suggested the potential and possibility for storage of lyophilized albumin nanoparticles over several months at 2-8 °C and even at 25 °C. Based on their findings, trehalose (as well as sucrose), were able to preserve the particle size and PDI over the course of 13 weeks, even at 40 °C. The method for freeze-drying of nab-mitotane (section **4.2.3**) was based on the freeze-drying process of HSA nanoparticles reported in this publication [51]. Thus, it is of great interest that nab-mitotane formulation can achieve stability over a longer period of time as reported for HSA nanoparticles [51].

5.2.3 Short-term stability study – summary

In summary, nab-mitotane was freeze-dried in the presence of 6% sucrose (w/v), and stored at room temperature and refrigerated temperature for 21 days. When assessing the influence of the lyophilization process on the particle size of the freeze-dried product, the nanoparticles remained stable with no significant changes in particle size or PDI. The resulting cake appearances after the lyophilization were mostly acceptable with the exception when product was visible around the opening of the vial. Rejection was due to impact on product quality. During the short-term stability study, freeze-dried nab-mitotane remained unchanged in particle diameter and PDI when stored at refrigerated temperature. However, a significant change occurred when the freeze-dried samples were stored at room temperature. Among the samples stored at room temperature, only the sample reconstituted on day 7 showed an increase in particle size, while PDI remained unchanged.

6 Conclusion and future work

In this study, the DC method utilized in the preparation of nab-mitotane were optimized. Prior to this project, the obtained particle size by DC had a mean of approx. 350 nm. As a mean to reduce the particle size, different parameters such as the size and amount of ceramic beads, processing temperature, processing time and the pH of the BSA solution were varied and assessed of their influence with respect to the particle size. Based on the results and supporting literature, the following parameters were selected for the preparation of nab-mitotane: 1200 mg ceramic beads with a diameter of 0.3-0.4 mm as homogenization aid, DC processing temperature at 20 °C for 60 min at a speed of 2350 rpm, and with BSA solution adjusted to pH 9. With these parameters, a mean particle size and PDI of 282.2 ± 9.2 nm and 0.119 ± 0.021 (n = 12) was achieved, respectively. By comparing the mean particle size of 282.2 nm with a theoretical mean of 350 nm in a one-sample t-test, the obtained particle size was considered significantly different from the reference ($p < 0.0001$). Thus, a particle size reduction was achieved. However, for future work, drug assay analysis should be conducted to determine the effect of particle size reduction on the drug concentration. Furthermore, a formulation optimization would be needed with an aim of producing nanoparticles of less than 200 nm in diameter that would be suitable for intravenous application. As a second option of interest, in order to optimize the nab-mitotane formulation, could be PEGylation of the nanoparticles to prevent rapid clearance from the circulation by opsonization [6, 75].

Additionally, lyophilization was carried out to get a first knowledge on how the particle size of nab-mitotane could be influenced by the exposure to stresses associated with freezing, dehydration and rehydration [53] in the presence of a cryoprotectant. Additionally, the intention of the short-term stability study was to gain a first knowledge of the extension in which the particle size of this formulation could be affected over time. Based on the results from the conducted study, this lyophilization method performed to lyophilize nab-mitotane was able to preserve the particle size and polydispersity at refrigerated temperature, at least for a short period of time. However, more experiments should be conducted for clarification of the stability when freeze-dried nab-mitotane are stored at room temperature. For future stability studies, a lyophilization cycle development would be necessary for improved preservation of nab-mitotane formulation in the final, dried state.

7 References

1. *Lysodren: EPAR – Scientific Discussion*. 2005 [cited 2021 December]; Available from: https://www.ema.europa.eu/en/documents/scientific-discussion/lysodren-epar-scientific-discussion_en.pdf.

2. Corso, C.R., et al., *Pharmacological profile and effects of mitotane in adrenocortical carcinoma.* British Journal of Clinical Pharmacology, 2021. **87**(7): p. 2698-2710.

3. Paragliola, R.M., et al., *Role of Mitotane in Adrenocortical Carcinoma - Review and State of the art.* European Endocrinology, 2018. **14**(2): p. 62-66.

4. *Mitotane*, in *LiverTox: Clinical and Research Information on Drug-Induced Liver Injury*. 2012, National Institute of Diabetes and Digestive and Kidney Diseases: Bethesda (MD).

5. Haider, M.S., et al., *The Challenging Pharmacokinetics of Mitotane: An Old Drug in Need of New Packaging.* European Journal of Drug Metabolism and Pharmacokinetics, 2021. **46**(5): p. 575-593.

6. Rizvi, S.A.A. and A.M. Saleh, *Applications of nanoparticle systems in drug delivery technology.* Saudi pharmaceutical journal : SPJ : the official publication of the Saudi Pharmaceutical Society, 2018. **26**(1): p. 64-70.

7. Macon, B.L. *Adrenal Cortical Carcinoma*. 2016 [cited 2021 November]; Available from: https://www.healthline.com/health/adrenocortical-carcinoma#types.

8. Sharma, E., et al., *The Characteristics and Trends in Adrenocortical Carcinoma: A United States Population Based Study.* Journal of clinical medicine research, 2018. **10**(8): p. 636-640.

9. Tkachenko, R., A. Golovko, and O. Kuryk, *A case report of late local relapse of adrenocortical carcinoma 18 years after adrenalectomy.* Experimental Oncology, 2018. **40**(3): p. 251-253.

10. Scheidt, H.A., et al., *The adrenal specific toxicant mitotane directly interacts with lipid membranes and alters membrane properties depending on lipid composition.* Molecular and Cellular Endocrinology, 2016. **428**: p. 68-81.

11. Libé, R., *Adrenocortical carcinoma (ACC): diagnosis, prognosis, and treatment.* Frontiers in Cell and Developmental Biology, 2015. **3**: p. 45-45.

12. Fassnacht, M., et al., *Adrenocortical carcinoma: a clinician's update.* Nature Reviews Endocrinology, 2011. **7**(6): p. 323-335.

13. Puglisi, S., et al., *New perspectives for mitotane treatment of adrenocortical carcinoma.* Best Practice & Research Clinical Endocrinology & Metabolism, 2020. **34**(3): p. 101415.

14. Chalasani, S., et al., *Metastatic virilizing adrenocortical carcinoma: a rare case of cure with surgery and mitotane therapy.* Clinical Medicine and Research, 2009. **7**(1-2): p. 48-51.

15. *Adrenal Gland Tumor: Statistics*. 2021 [cited 2021 November]; Available from: https://www.cancer.net/cancer-types/adrenal-gland-tumor/statistics.

16. *Adrenal Gland Tumor: Introduction*. 2021 [cited 2021 November]; Available from: https://www.cancer.net/cancer-types/adrenal-gland-tumor/introduction.

17. Pittaway, J.F.H. and L. Guasti, *Pathobiology and genetics of adrenocortical carcinoma.* Journal of Molecular Endocrinology, 2019. **62**(2): p. R105-r119.

18. Terzolo, M., et al., *Adjuvant Mitotane Treatment for Adrenocortical Carcinoma.* New England Journal of Medicine, 2007. **356**(23): p. 2372-2380.

19. Fassnacht, M., et al., *Combination Chemotherapy in Advanced Adrenocortical Carcinoma.* New England Journal of Medicine, 2012. **366**(23): p. 2189-2197.

20. Megerle, F., et al., *Advanced Adrenocortical Carcinoma – What to do when First-Line Therapy Fails?* Experimental and Clinical Endocrinology & Diabetes, 2018. **127**.

21. De Filpo, G., M. Mannelli, and L. Canu, *Adrenocortical carcinoma: current treatment options.* Current Opinion in Oncology, 2021. **33**(1).

22. *Mitotane*. 2005 [cited 2021 October]; Available from: https://go.drugbank.com/drugs/DB00648.

23. Yin, A., et al., *Population Pharmacokinetic and Pharmacogenetic Analysis of Mitotane in Patients with Adrenocortical Carcinoma: Towards Individualized Dosing.* Clinical Pharmacokinetics, 2021. **60**(1): p. 89-102.

24. Lo Iacono, M., et al., *Molecular Mechanisms of Mitotane Action in Adrenocortical Cancer Based on In Vitro Studies.* Cancers, 2021. **13**(21): p. 5255.

25. *Lysodren: EPAR – Product Information*. 2009 [cited 2021 December]; Available from: https://www.ema.europa.eu/en/documents/product-information/lysodren-epar-product-information_en.pdf.

26. Sbiera, S., et al., *Mitotane Inhibits Sterol-O-Acyl Transferase 1 Triggering Lipid-Mediated Endoplasmic Reticulum Stress and Apoptosis in Adrenocortical Carcinoma Cells.* Endocrinology, 2015. **156**(11): p. 3895-3908.

27. Tyagi, P. and J.A. Subramony, *Nanotherapeutics in oral and parenteral drug delivery: Key learnings and future outlooks as we think small.* Journal of Controlled Release, 2018. **272**: p. 159-168.

28. Rizvi, S.A.A. and A.M. Saleh, *Applications of nanoparticle systems in drug delivery technology.* Saudi Pharmaceutical Journal, 2018. **26**(1): p. 64-70.

29. Hoshyar, N., et al., *The effect of nanoparticle size on in vivo pharmacokinetics and cellular interaction.* Nanomedicine (London, England), 2016. **11**(6): p. 673-692.

30. Bridges, J., et al., *Scientific basis for the definition of the term «nanomaterial»*. 2012: Publications Office of the European Union. 46 pages.

31. Ventola, C.L., *Progress in Nanomedicine: Approved and Investigational Nanodrugs.* Pharmacy and Therapeutics: a Peer-Reviewed Journal for Formulary Management, 2017. **42**(12): p. 742-755.

32. *Nanoparticles could help us understand the relationship between structure and function in the brain*. 2019 [cited 2022 April]; Available from: https://escience.washington.edu/nanoparticles-could-help-us-understand-the-relationship-between-structure-and-function-in-the-brain/.

33. Donahue, N.D., H. Acar, and S. Wilhelm, *Concepts of nanoparticle cellular uptake, intracellular trafficking, and kinetics in nanomedicine.* Advanced Drug Delivery Reviews, 2019. **143**: p. 68-96.

34. Garbayo, E., et al., *Nanomedicine and drug delivery systems in cancer and regenerative medicine.* Wiley Interdisciplinary Reviews: Nanomedicine and Nanobiotechnology, 2020. **12**(5): p. e1637.

35. An, F.-F. and X.-H. Zhang, *Strategies for Preparing Albumin-based Nanoparticles for Multifunctional Bioimaging and Drug Delivery.* Theranostics, 2017. **7**: p. 3667-3689.

36. Ciruelos, E. and C. Jackisch, *Evaluating the role of nab-paclitaxel (Abraxane) in women with aggressive metastatic breast cancer.* Expert Review of Anticancer Therapy, 2014. **14**(5): p. 511-21.

37. Wang, R., P.S. Billone, and W.M. Mullett, *Nanomedicine in Action: An Overview of Cancer Nanomedicine on the Market and in Clinical Trials.* Journal of Nanomaterials, 2013. **2013**: p. 629681.

38. Cecco, S., et al., *Safety and efficacy evaluation of albumin-bound paclitaxel.* Expert Opinion on Drug Safety, 2014. **13**(4): p. 511-520.

39. Elzoghby, A.O., W.M. Samy, and N.A. Elgindy, *Albumin-based nanoparticles as potential controlled release drug delivery systems.* Journal of Controlled Release, 2012. **157**(2): p. 168-182.

40. Tong, R., et al., *The formulation of aptamer-coated paclitaxel-polylactide nanoconjugates and their targeting to cancer cells.* Biomaterials, 2010. **31**(11): p. 3043-3053.

41. Kudarha, R.R. and K.K. Sawant, *Albumin based versatile multifunctional nanocarriers for cancer therapy: Fabrication, surface modification, multimodal therapeutics and imaging approaches.* Materials Science and Engineering: C, 2017. **81**: p. 607-626.

42. Kratz, F., *Albumin as a drug carrier: Design of prodrugs, drug conjugates and nanoparticles.* Journal of Controlled Release, 2008. **132**(3): p. 171-183.

43. Ma, P. and R.J. Mumper, *Paclitaxel Nano-Delivery Systems: A Comprehensive Review.* Journal of Nanomedicine & Nanotechnology, 2013. **4**(2): p. 1000164-1000164.

44. Villaverde Cantizano, G. and A. Baeza, *Targeting strategies for improving the efficacy of nanomedicine in oncology.* Beilstein Journal of Nanotechnology, 2019. **10**: p. 168-181.

45. Bozzuto, G. and A. Molinari, *Liposomes as nanomedical devices.* International Journal of Nanomedicine, 2015. **10**: p. 975-99.

46. Hoogenboezem, E.N. and C.L. Duvall, *Harnessing albumin as a carrier for cancer therapies.* Advanced Drug Delivery Reviews, 2018. **130**: p. 73-89.

47. Chenthamara, D., et al., *Therapeutic efficacy of nanoparticles and routes of administration.* Biomaterials Research, 2019. **23**(1): p. 20.

48. Massing, U., et al., *Dual Centrifugation - A Novel "in-vial" Liposome Processing Technique*, in *Liposomes*, A. Catala, Editor. 2017, IntechOpen. p. 3-28.

49. Hagedorn, M., et al., *Dual centrifugation – A new technique for nanomilling of poorly soluble drugs and formulation screening by an DoE-approach.* International Journal of Pharmaceutics, 2017. **530**(1): p. 79-88.

50. Massing, U., S. Cicko, and V. Ziroli, *Dual asymmetric centrifugation (DAC)--a new technique for liposome preparation.* Journal of Controlled Release, 2008. **125**(1): p. 16-24.

51. Anhorn, M.G., H.-C. Mahler, and K. Langer, *Freeze drying of human serum albumin (HSA) nanoparticles with different excipients.* International Journal of Pharmaceutics, 2008. **363**(1): p. 162-169.

52. Ó'Fágáin, C., *Lyophilization of Proteins*, in *Protein Purification Protocols*, P. Cutler, Editor. 2004, Humana Press: Totowa, NJ. p. 309-321.

53. Mohammady, M., Y. mohammadi, and G. Yousefi, *Freeze-Drying of Pharmaceutical and Nutraceutical Nanoparticles: The Effects of Formulation and Technique Parameters on Nanoparticles Characteristics.* Journal of Pharmaceutical Sciences, 2020. **109**(11): p. 3235-3247.

54. Snape, T.J., A.M. Astles, and J.A. Davies, *Understanding the chemical basis of drug stability and degradation.* The Pharmaceutical Journal, 2010. **285**: p. 416-417.

55. Tattini, V., et al., *Effect of lyophilization on the structure and phase changes of PEGylated-bovine serum albumin.* International Journal of Pharmaceutics, 2005. **304**(1): p. 124-134.

56. *Smart Freeze Drying: Basic principles, optimum procedures and applications*. 2015 [cited 2022 January]; Available from: https://www.martinchrist.de/fileadmin/user_upload/christ/04_anwendungen/lyophilisation/Smart_FD_Basics_Apps_en.pdf.

57. Aulton, M. and K. Taylor, *Aulton's Pharmaceutics: the Design and Manufacture of Medicines*. 2018: Elsevier.

58. *The lyophilization process* [cited 2022 March]; Available from: https://www.labogene.com/The-Lyophilization-Process.

59. Hottot, A., S. Vessot, and J. Andrieu, *A Direct Characterization Method of the Ice Morphology. Relationship Between Mean Crystals Size and Primary Drying Times of Freeze-Drying Processes.* Drying Technology, 2004. **22**: p. 2009-2021.

60. Bisht, D. and Z. Iqbal, *Lyophilization - process and optimization for pharmaceuticals.* International Journal of Drug Regulatory Affairs, 2018. **3**: p. 30-40.

61. Horn, J. and W. Friess, *Detection of Collapse and Crystallization of Saccharide, Protein, and Mannitol Formulations by Optical Fibers in Lyophilization.* Frontiers in Chemistry, 2018. **6**: p. 4-4.

62. Tang, X. and M.J. Pikal, *Design of freeze-drying processes for pharmaceuticals: practical advice.* Pharmaceutical Research, 2004. **21**(2): p. 191-200.

63. Barley, J. *Basic Principles of Freeze Drying*. [cited 2022 February]; Available from: https://www.spscientific.com/freeze-drying-lyophilization-basics/.

64. Abdelwahed, W., et al., *Freeze-drying of nanoparticles: Formulation, process and storage considerations.* Advanced Drug Delivery Reviews, 2006. **58**(15): p. 1688-1713.

65. Patel, S.M., et al., *Lyophilized Drug Product Cake Appearance: What Is Acceptable?* Journal of Pharmaceutical Sciences, 2017. **106**(7): p. 1706-1721.

66. Langer, K., et al., *Optimization of the preparation process for human serum albumin (HSA) nanoparticles.* International Journal of Pharmaceutics, 2003. **257**(1): p. 169-180.

67. Shokri, M., M. Tavallaie, and M. Hosseini, *Effect of Lyophilization on the Size and Polydispersity of Unilamellar and Multilamellar Liposomes.* Journal of Nanotechnology and Materials Science, 2016. **3**: p. 1-4.

68. Chen, C., et al., *An overview of liposome lyophilization and its future potential.* Journal of Controlled Release, 2010. **142**(3): p. 299-311.

69. Burden, D., H. Brangs, and L. Gibbons, *Bead Beating: A Primer*. 2014, USA: OPS Diagnostics LLC.

70. *Interpreting results: Two-way ANOVA*. [cited 2022 May]; Available from: https://www.graphpad.com/guides/prism/latest/statistics/how_to_think_about_results_from_two-way_anova.htm.

71. Steiner, D. and H. Bunjes, *Influence of process and formulation parameters on the preparation of solid lipid nanoparticles by dual centrifugation.* International Journal of Pharmaceutics: X, 2021. **3**: p. 100085.

72. Johnson, S. *Science Project: The Effects of Temperature on Liquids*. [cited 2022 May]; Available from: https://sciencing.com/science-project-effects-temperature-liquids-7796706.html.

73. *BSA*. [cited 2022 May]; Available from: https://www.prospecbio.com/bovine_serum_albumin.

74. *Protein stability and storage*. 2009 [cited 2022 May]; Available from: https://tools.thermofisher.com/content/sfs/brochures/TR0043-Protein-storage.pdf.

75. Shi, L., et al., *Effects of polyethylene glycol on the surface of nanoparticles for targeted drug delivery.* Nanoscale, 2021. **13**(24): p. 10748-10764.

8 Appendix

Appendix I

Table S1: *Ice-vapor pressure chart. Temperature and pressure on the curve allowing sublimation [56].*

Tempera-ture (°C)	Pressure (mbar)	Tempera-ture (°C)	Pressure (mbar)	Tempera-ture (°C)	Pressure (mbar)	Tempera-ture (°C)	Pressure (mbar)	Tempera-ture (°C)	Pressure (mbar)
0	6.110	-12	2.170	-24	0.700	-36	0.200	-48	0.050
-1	5.620	-13	1.980	-25	0.630	-37	0.180	-49	0.045
-2	5.170	-14	1.810	-26	0.570	-38	0.160	-50	0.040
-3	4.760	-15	1.650	-27	0.520	-39	0.140	-51	0.035
-4	4.370	-16	1.510	-28	0.470	-40	0.120	-52	0.030
-5	4.020	-17	1.370	-29	0.420	-41	0.110	-53	0.025
-6	3.690	-18	1.250	-30	0.370	-42	0.100	-54	0.024
-7	3.380	-19	1.140	-31	0.340	-43	0.090	-55	0.021
-8	3.010	-20	1.030	-32	0.310	-44	0.080	-56	0.018
-9	2.840	-21	0.940	-33	0.280	-45	0.070	-57	0.016
-10	2.560	-22	0.850	-34	0.250	-46	0.060	-58	0.014
-11	2.380	-23	0.770	-35	0.220	-47	0.055	-59	0.012

Appendix II – Dual centrifugation: statistical data (p-values)

The tables below show the adjusted p-values provided by a post hoc test following a significant ANOVA analysis.

The influence of different amounts of ceramic beads on particle size

Table S 2: *Tukey's post hoc test comparing mean particle sizes and PDIs between groups with different amounts of ceramic beads (Ø: 0.3-0.4 mm).*

Statistical significance		
One-way ANOVA + Tukey's post hoc test		
Groups	**Adjusted p-value (particle size)**	**Adjusted p-value (PDI)**
300 mg and 750 mg	< 0.0001 (****)	0.0006 (***)
300 mg and 1200 mg	0.1646 (ns)	0.3133 (ns)
750 mg and 1200 mg	< 0.0001 (****)	0.0032 (**)
Statistical significance summary: **** p ≤ 0.0001; *** p ≤ 0.001; ** p ≤ 0.01; * p ≤ 0.05; ns p > 0.05. Alpha = 0.05		

Table S 3: *Bonferroni's multicomparisons test comparing mean particle sizes and PDIs based on groups with different sizes and different amounts of ceramic beads.*

Statistical significance		
Two-way ANOVA + Bonferroni's multicomparisons test		
Groups (amounts of ceramic beads (mg))	**Adjusted p-value (particle size)**	**Adjusted p-value (PDI)**
300	0.0222 (*)	0.0055 (**)
1200	< 0.0001 (****)	0.0847 (ns)
Statistical significance summary: **** p ≤ 0.0001; *** p ≤ 0.001; ** p ≤ 0.01; * p ≤ 0.05; ns p > 0.05. Alpha = 0.05		

The influence of temperature on the particle size

Table S 4: *Tukey's post hoc test comparing mean particle sizes and PDIs between groups of nab-mitotane prepared at different temperatures.*

Statistical significance		
One-way ANOVA + Tukey's post hoc test		
Groups	**Adjusted p-value (particle size)**	**Adjusted p-value (PDI)**
5 °C and 15 °C	0.0072 (**)	0.0116 (*)

5 °C and 20 °C	0.0023 (**)	0.0020 (**)
5 °C and 25 °C	0.0033 (**)	0.0002 (***)
5 °C and 40 °C	0.0007 (***)	< 0.0001 (****)
15 °C and 20 °C	0.9242 (ns)	0.7386 (ns)
15 °C and 25 °C	0.9814 (ns)	0.0849 (ns)
15 °C and 40 °C	0.464 (ns)	0.0047 (**)
20 °C and 25 °C	0.9987 (ns)	0.4627 (ns)
20 °C and 40 °C	0.8831 (ns)	0.0296 (*)
25 °C and 40 °C	0.7591 (ns)	0.3737 (ns)
Statistical significance summary: **** $p \leq 0.0001$; *** $p \leq 0.001$; ** $p \leq 0.01$; * $p \leq 0.05$; ns $p > 0.05$. Alpha = 0.05		

Appendix III – Experimental: Sucrose as cryoprotectant

The influence of different sucrose concentrations on the particle size

The sucrose concentrations chosen for this experiment were based on a study conducted by Anhorn et al. [51] and colleagues. In their study, they investigated different concentrations of sucrose, trehalose, and mannitol (w/v) as potential cryoprotectants for freeze-drying of HSA nanoparticle suspensions. The article concluded that 2-3% sucrose or trehalose resulted in optimal preservation of particle diameter and polydispersity of nanoparticles (HSA, 10 mg/mL) by preventing aggregation that are usually associated with freeze-drying and subsequent reconstitution. In this experiment, 2, 4, 6, and 8% sucrose (w/v) were used as cryoprotectant for comparison. The results in form of particle size and PDI obtained before and after lyophilization are shown in **Figure S 1**.

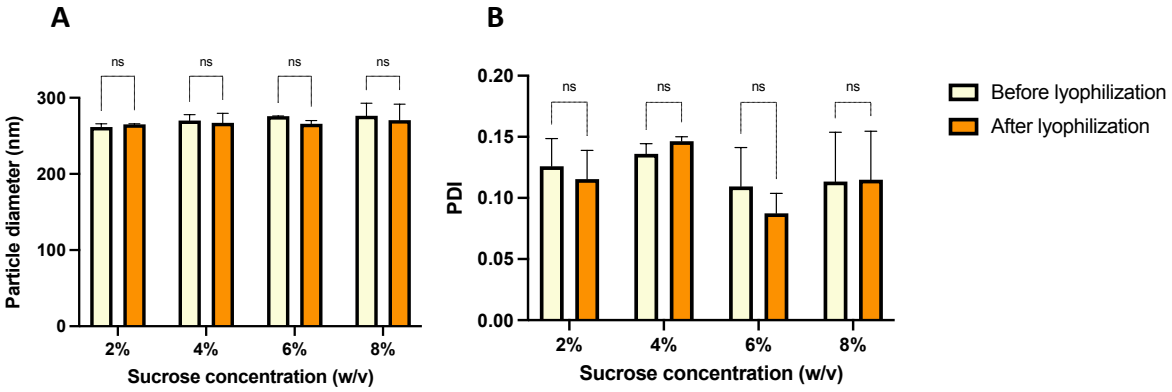

Figure S 1: A) *Mean particle size and* ***B)*** *mean PDI of nab-mitotane comparing a control group (before lyophilization) with groups of different concentrations of sucrose (w/v) (mean ± SD, n = 2). Statistical significance displayed as **** p ≤ 0.0001; *** p ≤ 0.001; ** p ≤ 0.01; * p ≤ 0.05; ns p > 0, 05. Alpha = 0.05.*

A two-way ANOVA and Bonferroni's multicomparisons test was performed to compare the different sucrose concentrations and to determine which was most suitable for the lyophilization of nab-mitotane. However, as stated in **Figure S 1**, there was no significant differences between the results obtained from before- and after lyophilization when comparing the use of 2, 4, 6 and 8% sucrose, respectively. Despite this, 6% sucrose was chosen due to a narrower size-distribution range (**Figure S 1B**).

Appendix IV – Lyophilization: statistical data (p-value)

The table below show the adjusted p-values provided by a post hoc test following a significant ANOVA analysis.

Stability after storage at room temperature

Table S 5: *Dunnett's post hoc test comparing both mean particle sizes and PDIs between the control group (reconstituted day 0) and groups that was stored and reconstituted at different timepoints.*

Statistical significance		
One-way ANOVA + DUNNETT's post hoc test		
Groups (control: day 0)	**Adjusted p-value (particle size)**	**Adjusted p-value (PDI)**
Day 1	0.7327 (ns)	0.9154 (ns)
Day 7	0.0296 (*)	0.7440 (ns)
Day 14	0.9702 (ns)	0.1466 (ns)
Day 21	0.8319 (ns)	0.5371 (ns)
Statistical significance summary: **** $p \leq 0.0001$; *** $p \leq 0.001$; ** $p \leq 0.01$; * $p \leq 0.05$; ns $p > 0.05$. Alpha = 0.05		